


Effects of Bisphenol A and Retinoic Acid Exposure on Neuron and Brain Formation: A Study in Human Induced Pluripotent Stem Cells and Zebrafish Embryos

Tomomi Nishie,¹ Tomoki Taya,¹ Shunichi Omori,¹ Kenya Ueno,² Yoshinori Okamoto,³ Shogo Higaki,^{1†} Marina Oka,¹ Yachiyo Mitsuishi,^{1‡} Taiga Tanaka,¹ Mana Nakamoto,¹ Hideaki Kawahara,¹ Natsuki Teraguchi,¹ Tomoyuki Kotaka,¹ Misaki Sawabe,¹ Miu Takahashi,¹ Shoko Kitaike,¹ Minori Wada,¹ Keiko Iida,² Akihiro Yamashita,⁴ Hideto Jinno,³ Atsuhiko Ichimura,¹ Ikuo Tooyama,⁵ Noriyoshi Sakai,⁶ Masahiko Hibi,⁷ Akira Hirasawa,² and Tatsuyuki Takada¹ 

¹Department of Pharmaceutical Sciences, Ritsumeikan University, Shiga, Japan

²Department of Genomic Drug Discovery Science, Graduate School of Pharmaceutical Sciences, Kyoto University, Kyoto, Japan

³Faculty of Pharmacy, Meijo University, Nagoya, Japan

⁴Department of Biochemistry and Molecular Biology, Faculty of Medicine, Osaka University, Osaka, Japan

⁵Molecular Neuroscience Research Center and Medical Innovation Research Center, Shiga University of Medical Science, Shiga, Japan

⁶Department of Gene Function and Phenomics, National Institute of Genetics, Mishima, Japan

⁷Graduate School of Science, Nagoya University, Nagoya, Japan

BACKGROUND: Developing human fetuses may be exposed to the chemical compound bisphenol A (BPA), and retinoic acid (RA) has been detected at low levels in water sources. RA signaling regulates key developmental genes and is essential for organ development, including the brain. We previously reported that RA/BPA coexposure of mouse embryonic stem cells potentiates RA signaling, which warrants further investigation.

OBJECTIVE: This study was undertaken in human induced pluripotent stem cells (iPSCs) and zebrafish embryos to investigate whether coexposure to BPA and exogenous RA could potentiate *HOX* gene expression and exert pleiotropic effects on RA signaling.

METHODS: Human iPSCs and zebrafish embryos were exposed to exogenous RA (0, 7.5, 10, 12.5, 100, 200 or 500 nM) or BPA (20 μ M) alone or coexposed to BPA (2 nM–20 μ M) and exogenous RA (7.5–100 nM). Postexposure changes in *HOX* genes were assessed by quantitative polymerase chain reaction and/or transcriptome analyses. RA receptor antagonists were used to identify the receptor responsible for signaling. In zebrafish, spatial expression of *fgf8a* and *hoxb1a* was evaluated by whole-mount *in situ* hybridization. Mauthner cell and craniofacial cartilage anomalies were studied by immunostaining and Alcian blue staining, respectively. Transcriptome was compared between iPSCs and zebrafish to identify alterations of common biological processes. Gradient curves of RA signal were calculated to simulate the effects of exogenous RA and BPA in zebrafish.

RESULTS: In both iPSCs and zebrafish, RA/BPA coexposure had higher expression of 3' *HOX* genes in comparison with RA alone; BPA alone had no effect. Addition of RA receptor antagonists abolished these changes. In zebrafish, RA/BPA coexposure, in comparison with RA alone, resulted in a significant rostral shift in *hoxb1a* expression and increased rate of anomalies in Mauthner cells and craniofacial cartilage. Transcriptome comparison and correlations between the experimental results and gradient curve simulations strengthened these observations.

CONCLUSION: Our findings suggest a mechanistic link between chemical exposure and neurodevelopmental impairments and demonstrate involvement of exogenous RA signaling in endocrine disruption. Further investigation is needed to explore why BPA alone did not affect endogenous RA signaling, whereas exogenous RA signaling was potentiated with RA/BPA coexposure. <https://doi.org/10.1289/EHP15574>

Introduction

Modern society heavily relies on synthetic chemicals and plastics, which are indispensable to daily life. Bisphenol A (BPA) is one of the highest-volume synthetic chemicals and is widely used to manufacture polycarbonate plastics and epoxy resins.^{1,2} It is found in numerous daily products, including water bottles, food containers, polyvinyl chloride films, dental sealants, and thermal paper. Studies have detected BPA in human serum¹; adipose tissue³; and brain, liver, and urine.⁴ In addition, BPA has been found in human placenta,¹ follicular fluid, amniotic fluid, breast milk of pregnant woman, and fetuses,⁵ suggesting that exposure

to BPA can occur during early gestational development. Furthermore, an impact on dopamine neurons,⁶ reproductive organs,⁷ and gene expression⁸ following prenatal exposure to BPA has been reported.

BPA interacts with multiple steroid hormone receptors, including estrogen, androgen, and thyroid receptors,⁹ and causes damage to the reproductive system, immune system, and neuroendocrine system,¹⁰ possibly by interfering with various cell signaling pathways.¹¹ However, a considerable knowledge gap exists regarding the adverse effects of BPA on the functions of hormone receptors, particularly because its mechanisms of action in a wide range of

Address correspondence to Akira Hirasawa, Department of Genomic Drug Discovery Science, Graduate School of Pharmaceutical Sciences, Kyoto University, Kyoto, Japan. Telephone: +81-75-753-4543; Fax: +81-75-753-4544. Email: hirasawa.akira.7v@kyoto-u.ac.jp. And, Tatsuyuki Takada, Laboratory of Cell Engineering, Department of Pharmaceutical Sciences, Ritsumeikan University, Nojihigashi 1-1-1, Kusatsu, Shiga 525-8577, Japan. Telephone: +81-77-561-2569; Fax: +81-77-561-2569. Email: ttakada@ph.ritsumei.ac.jp.

Supplemental Material is available online (<https://doi.org/10.1289/EHP15574>).

†Current address: Shogo Higaki, National Agriculture and Food Research Organization, National Institute of Animal Health, Tsukuba, Japan.

‡Current address: Yachiyo Mitsuishi, Molecular Neuroscience Research Center and Medical Innovation Research Center, Shiga University of Medical Science, Shiga, Japan.

The authors report no conflicts of interest.

Conclusions and opinions are those of the individual authors and do not necessarily reflect the policies or views of EHP Publishing or the National Institute of Environmental Health Sciences.

EHP is a Diamond Open Access journal published with support from the NIEHS, NIH. All content is public domain unless otherwise noted. Contact the corresponding author for permission before any reuse of content. [Full licensing information](#) is available online.

Received 14 June 2024; Revised 25 December 2024; Accepted 1 May 2025; Published 13 June 2025.

Note to readers with disabilities: *EHP* strives to ensure that all journal content is accessible to all readers. However, some figures and Supplemental Material published in *EHP* articles may not conform to 508 standards due to the complexity of the information being presented. If you need assistance accessing journal content, please contact ehpsubmissions@niehs.nih.gov. Our staff will work with you to assess and meet your accessibility needs within 3 working days.

disorders remain incompletely understood. This gap is partly attributed to the fact that experiments have been conducted under extensively divergent conditions, both *in vivo* and *in vitro*, using different animals, tissues, cell types, chemical concentrations, exposure durations, and analytical methods. Thus, integrating the diverse results of these experiments and deducing a common mechanism underlying adverse outcomes from exposure to endocrine-disrupting chemicals (EDCs) remain challenging.

Performing experiments focused on specific signaling under simplified and well-defined conditions is crucial to understanding the mechanisms underlying these effects.^{12,13} Research on EDCs has mainly focused on their effects on sex and steroid hormone receptors, with a particular focus on estrogenic potency.¹⁴ However, emerging evidence has demonstrated that their adverse effects extend beyond hormonal pathways, with studies showing an impact of EDCs on neurodevelopmental disorders such as autism spectrum disorder (ASD) and attention deficit hyperactivity disorder (ADHD) as well as effects on metabolism, obesity, developmental processes, immune systems, and epigenesis.^{12,15} These findings imply that EDCs, including BPA, might interfere with not only hormone receptors but also fundamental biological processes associated with early development.^{13,15}

We previously reported that mouse embryonic stem cells coexposed to BPA and retinoic acid (RA) had a higher expression of RA-responsive genes, including *Hoxa1*, in comparison with those exposed to RA alone.¹⁶ Because RA signaling plays fundamental roles in various developmental processes, including reproduction, immunity, carcinogenesis, and homeostasis, interference with the retinoid system could be linked to a diverse range of health disorders.^{17,18}

The presence of RA and RA-like activity was detected in drinking water sources.^{19–23} The main source of retinoids in surface water is cyanobacteria bloom and wastewater effluent. Retinoid-like activities have been detected in studies using a receptor-mediated *in vitro* bioassay or liquid chromatography–tandem mass spectrometry (LC-MS/MS), with the maximum activity of retinoids in surface water reported to be 263 ng/L all-*trans*-RA equivalent.²⁰ Studies of an effluent from a sewage treatment plant demonstrated the coexistence of BPA (1,225–2,638 ng/L as EDCs) and RA (3.7–9.1 ng/L) in the effluent.²¹

Both the Swedish Chemicals Agency and the European Commission have begun to focus on the susceptibility of the retinoid system to endocrine disruption.¹³ The pleiotropic effect of BPA suggests that it interferes with RA signaling, which acts as a morphogen during embryonic development and plays a key role in many fundamental biological processes. However, no direct evidence has been presented to indicate that food-contact chemicals interfere with RA signaling, and the molecular mechanism underlying this pleiotropic effect is poorly understood.

In this study, we focused on the effect of exogenous RA and RA/BPA coexposure in experiments using human induced pluripotent stem cells (iPSCs) and zebrafish embryos. These experiments sought to demonstrate that coexposure to exogenous RA and BPA may potentiate RA signaling and could be associated with the development of neurodevelopmental impairments.

Methods

Chemicals

All chemicals used in the experiments (product numbers, sources, purity, and Chemical Abstracts Service Numbers) are listed in Table S1. These chemicals include all-*trans*-RA, dimethyl sulfoxide (DMSO), BPA, mitomycin C, L-alanyl-L-glutamine, BMS493, AM580, LE135, BMS195614, G-15, LY2955303,

β-mercaptoethanol, ICI 182,780, and 4-nonylphenol (NP). All of the chemicals were dissolved in DMSO to prepare stock solutions and stored at –25°C. Working solutions were prepared by further dilution of the stock solutions. DMSO was used as the vehicle control.

Culture of Human iPSCs and Chemical Treatments

Human iPSCs (409B2, RBRC-HPS0076; RIKEN) were maintained on mitomycin C–treated SNL76/7 feeder cells (No. EC07032801; Cosmo Bio) cultured as a monolayer on gelatin-coated 6-cm dishes in maintenance medium, consisting of Dulbecco's modified Eagle's medium/Ham's F-12 (No. 08460-95; Nacalai Tesque) supplemented with 20% KnockOut Serum Replacement (No. 10828028; Thermo Fisher Scientific), 2 mM L-alanyl-L-glutamine, 0.11 mM β-mercaptoethanol, 1% nonessential amino acids (No. 06344-56; Nacalai Tesque), 5 ng/mL human recombinant basic fibroblast growth factor (hbFGF) (No. 064-04541; Wako Pure Chemical Industries), and 0.5% penicillin–streptomycin (No. 26253-84; Nacalai Tesque). The SNL76/7 cells were treated with 12 μg/mL mitomycin C for 2.25 h, cryopreserved in liquid nitrogen, and plated at a density of 8×10^5 cells per 6-cm dish within 1 or 2 d prior to iPSC plating. The iPSCs were obtained at passage 29, with a confirmed normal female karyotype (46 XX) at passage 25, and used for experiments between passages 36 and 46.

We applied the differentiation method,^{24,25} with slight modifications, to induce neuroectoderm and *HOX* genes. The human iPSCs initially cultured on SNL76/7 feeder cells were transferred to feeder-free conditions using E8 medium (No. A1517001; Thermo Fisher Scientific). After 4 d, the cells were reseeded onto 24-well plates at a density of 1.5×10^5 cells/well. The next day, the medium was replaced with 1 mL of E6 medium (No. A1516401; Thermo Fisher Scientific), and chemical treatments were initiated for 3 d. The medium was refreshed daily, and cells were harvested on the fourth day post treatment.

For RA treatment, a 1 μM working solution was prepared by diluting (1:1,000) a 1 mM RA stock (in DMSO) with E6 medium. To achieve a final concentration of 100 nM, 100 μL of the 1 μM working solution was added to make a final volume of 1 mL of medium. Other chemicals, such as BPA, were prepared as 10,000× diluted stock and added in a similar manner. For RA/BPA coexposure, RA was added first, followed immediately by BPA. In control cultures, DMSO (0.2% final concentration) was used.

Reverse Transcription–Quantitative Polymerase Chain Reaction

Total RNA was extracted directly from cells in wells using the ReliaPrep RNA Cell Miniprep System (No. X6011; Promega) according to the manufacturer's protocol. RNA concentration was measured with a BioDrop spectrophotometer (Berthold). Reverse transcription (RT) was performed with 250 ng of total RNA using the PrimeScript RT reagent kit (No. RR037A; Takara Bio).

RT-quantitative polymerase chain reaction (RT-qPCR) was conducted using SYBR Premix EX Taq (No. RR820A; Takara Bio) or TaqMan Fast Advanced Master Mix (No. 4444556; Thermo Fisher Scientific) on a StepOnePlus Real-Time PCR System or QuantStudio 5 (Thermo Fisher Scientific). Gene expression was normalized to *GAPDH*, calculated using the comparative threshold cycle (C_t) method.

PCR cycling conditions were as follows: for SYBR, 95°C for 30 s, followed by 40 cycles of 5 s at 95°C and 30 s at 60°C; for TaqMan, 95°C for 20 s, followed by 40 cycles of 1 s at 95°C and 20 s at 60°C. Relative expression levels were calculated using the

2^{−ΔΔCt} method. Each sample was analyzed in technical triplicate. Primers were obtained from Eurofins Genomics and Thermo Fisher Scientific, as detailed in Table S2.

Microarray Analysis of Human iPSCs

Microarray analysis of iPSCs was performed using total RNA as described above ($n = 3$ samples/group). Genome-wide messenger RNA expression profiles were obtained using the HuGene 2.0 ST Array (Affymetrix) following the manufacturer's instructions. Normalized data are available in the GEO database (Accession No. GSE263569).

Data analysis and visualization were conducted using R (version 4.2; R Development Core Team) and Bioconductor (version 3.16).²⁶ Expression levels were derived from probe intensities, normalized across all 18 samples using the Robust multiarray analysis (RMA) method.²⁷ Probe sets with normalized signals >20 were considered to indicate gene expression, and these probe sets were included in further analysis. Differentially expressed genes (DEGs) were identified using Welch's analysis of variance (ANOVA) ($p < 0.05$), implemented with the Bioconductor package GeneFilter. R scripts used for analysis are publicly available at <https://github.com/gpr120/hiPSC-Zebrafish-exprs>.

Immunohistochemistry and Flow Cytometry

After chemical treatment, cells were washed with phosphate-buffered saline (PBS) and fixed with 2% paraformaldehyde (PFA). Fixed cells were permeabilized with 0.3% Triton X-100, blocked with 2% bovine serum albumin (BSA), and incubated with HOXB1 antibody (diluted 1:100; No. AF6318; R&D Systems) for 3 h at room temperature. After washing twice with PBS, Alexa Fluor 488-conjugated goat anti-rabbit IgG (diluted 1:1,000; No. A-11008; Thermo Fisher Scientific) was added, followed by incubation for 45 min.

For flow cytometry, cells were dissociated using TrypLE Express (No. 12604013; Thermo Fisher Scientific), followed by fixation, permeabilization, and antibody staining as described above. Stained cells were filtered through a 40- μ m nylon mesh (No. N-N0330T; NBC Meshtec), resuspended in PBS with 1% BSA, and analyzed using a FACSCalibur flow cytometer (BD Biosciences). Data were processed with CellQuest Pro software (version 6.0; BD Biosciences).

Fish Husbandry and Chemical Treatments

All experiments with zebrafish embryos were approved by the Committee on Laboratory Animal Care and Use at Ritsumeikan University (Approval No. BKC2020-048) and conducted in accordance with the university's guidelines. Wild-type zebrafish (*Danio rerio*, strain RIKEN WT) were obtained from RIKEN BRC and maintained under a 12-h light/12-h dark photoperiod at $28 \pm 1^\circ\text{C}$. Embryos were collected 30 min post mating [0.5 hours post fertilization (hpf)] and grown at 28°C in E3 embryo medium (5 mM NaCl, 0.17 mM KCl, 0.33 mM CaCl_2 , 0.33 mM MgSO_4 , 10 mM HEPES, pH 7.22).

RA, BPA, LE135, and NP solutions were prepared ~ 1 h before use. A 12.5- μM RA solution was prepared in DMSO from a 1-mM stock, followed by stepwise dilution with E3 to prepare 12.5-nM, 10-nM, and 7.5-nM solutions. For co-treatments, 3 mL of RA solution was mixed with 1,000 \times diluted concentrations of BPA (20 mM), LE135 (10 μM), or NP (10 μM), to achieve final concentrations of 20 μM and 10 nM for each treatment.

A total of 60 embryos were distributed into 35-mm dishes (No. 1-8459-01; AsOne) containing 3 mL of E3 medium. Embryos at the 4–8-cell stage were treated with chemicals by replacing E3 with 3 mL of chemical-containing E3, and the

embryos were then incubated until 24 hpf at 28°C . Control embryos were incubated in E3 containing 0.2% DMSO. At 24 hpf, the medium was replaced with fresh E3 without chemicals, and the embryos were incubated until the desired stages for sampling.

For immunostaining, embryos were treated with 0.03 mg/mL 1-phenyl-2-thiourea (PTU) (No. 166-13702; Wako) between 24 and 48 hpf, to inhibit melanocyte production.

LC-MS/MS Quantification of All-trans-RA in Culture Medium and Embryos

Concentrations of RA in the prepared samples of culture medium, and embryos were measured using LC-MS/MS, with minor modifications to a previously described method.²⁸ Culture medium (100 μL per sample) and 10 embryos per group were collected at 0, 2, 5, 9, and 23 h post exposure to RA (0, 7.5, 10, or 12.5 nM), BPA (20 μM), or combinations of RA (7.5 or 10 nM) and BPA (20 μM) ($n = 3$ samples per group). Embryos were homogenized in E3 medium (10 embryos/100 μL) and mixed with 400 μL methanol containing 1.25 nM RA-d5 (No. 25415; Cayman Chemicals) as an internal standard. After centrifugation (15,000 rpm for 10 min at 4°C), supernatants were transferred to high-performance LC vials for LC-MS/MS analysis.

LC separation was performed using ultra-high performance liquid chromatography (UHPLC; Exion LC system; Sciex) with a reverse-phase column (InertCore Plus C18, 3.0×100 mm, $\phi 2.6$ μm ; GL Sciences Inc.) under the following conditions: flow rate, 0.8 mL/min; column temperature, 40°C ; injection volume, 50 μL ; mobile phase A, 0.1% formic acid in water; mobile phase B, 100% methanol. The gradient was started at 80% B, increased linearly to 98% B at 4 min, held for 1 min, and reequilibrated over 1 min, for a total runtime of 6 min. RA and RA-d5 were eluted at 2.81 min and 2.80 min, respectively.

Detection of RA was conducted using a QTRAP 6500+ triple-quadrupole mass spectrometer (Sciex) with an electrospray ionization (ESI) source in positive ion mode. ESI parameters were as follows: turbo gas temperature, 300°C ; ion source voltage, 5,500 V; curtain gas, 40 psi; nebulizer gas (GS1), 70 psi; heater gas (GS2), 50 psi; collision gas, 8 psi. Multiple reaction monitoring (MRM) conditions are detailed in Table S3.

LC-MS/MS data were acquired using Analyst software (version 1.7.2; Sciex) and quantified with Sciex OS-Q software (version 2.1.6; Sciex).²⁸

Whole-Mount In Situ Hybridization of Fish Embryos

Zebrafish embryos (24 hpf) ($n = 20$ –30/group) were fixed with 4% PFA overnight and dehydrated by methanol after physical dechoriation using a 27G needle. Whole-mount *in situ* hybridization (WISH) was performed as previously described.²⁹ Digoxigenin (DIG)– or fluorescein isothiocyanate (FITC)–labeled antisense RNA probes (for *fgf8a*, *hoxb1a*, *otx2b*, *egr2a*, *hoxb4a*, *hoxb5a*, and *cyp26a1*) were synthesized using a DIG RNA labeling kit (SP6/T7, No. 11175025910; Roche) and Fluorescein RNA labeling mix (No. 11685619910; Roche). The embryos were photographed using a stereomicroscope (Nikon SMZ800N) equipped with a complementary metal-oxide-semiconductor (CMOS) camera (Wraymer Floyd digital microscope camera). The distance between signals was measured in lateral-view embryos using Image J (version 1.53a). The probe sequences are listed in Table S4.

Whole-Mount Immunostaining of Fish Neuronal Cells

Zebrafish Mauthner neuronal cells (M-cells) were visualized by immunostaining using 48 hpf embryos ($n = 20$ embryos per group). Embryos were fixed with 2% trichloroacetic acid for 3 h

at room temperature (20°–24°C) and dechorionated manually as described above.

Embryos were blocked with 10% normal goat serum and 0.1% BSA in PBS–Tween (PBS-T) and then immunostained overnight at 4°C with anti-NEFM monoclonal antibody (RMO-44, SC248186; Thermo Fisher Scientific) at 1:100 dilution. After washing with PBS-T, embryos were incubated with Alexa 488–conjugated antimouse IgG (Thermo Fisher Scientific) at 1:500 dilution. Embryos were washed with PBS-T and photographed using a CMOS camera (Wraymer Floyd).

Alcian Blue Staining of Fish Cartilage

Cartilage from zebrafish embryos at 96 hpf was stained with Alcian blue, as previously described.³⁰ In brief, embryos (larvae) ($n = 20$ per group) were fixed with 4% PFA and stained overnight with Alcian blue solution (No. 37154-44; Nacalai Tesque). After washing with PBS, larvae were treated with 0.05% trypsin/PBS-T for 2 h, followed by bleaching in 1.5% H₂O₂ per 1% KOH solution and then clearing in deionized water overnight.

All embryos were photographed, and images were analyzed using Image J software (version 1.53a). Neurocranium formation in the embryos was quantified by measuring the anteroposterior length of the ethmoid plate and trabeculae (tr), from the rostral tip of the ethmoid plate to the occipital arch (oa), and angles [Meckel's palatoquadrate (M-PQ) and ceratohyal cartilage (CH)].^{30,31}

Statistical Analysis

All statistical analyses were conducted using R (version 4.2.1; R Development Core Team). Arcsine square root transformation of the percentage data was applied to normalize the variance before analysis. A one-way ANOVA with Tukey's multiple comparisons test was employed to compare the different groups on all pairwise combinations. An ANOVA with Dunnett's multiple comparisons test was employed to compare the different groups to the control group. Welch's *t*-tests were used to analyze comparisons between two groups. A *p*-value < 0.05 was considered statistically significant. Data are presented as mean ± standard deviation (SD), unless otherwise specified.

Mathematical Simulation with RA Gradient Curves

The RA gradient model was defined as the following one-dimensional reaction-diffusion model, as reported by White et al.³²

$$\frac{\partial[\text{RA}]_{\text{out}}}{\partial t} = D \frac{\partial^2[\text{RA}]_{\text{out}}}{\partial x^2} + V(x) - (1 + \beta)k_p[\text{RA}]_{\text{out}} + k_p[\text{RA}]_{\text{in}} \quad (1)$$

$$\frac{\partial[\text{RA}]_{\text{in}}}{\partial t} = k_p[\text{RA}]_{\text{out}} - (k_p + [\text{Cyp}])[\text{RA}]_{\text{in}} \quad (2)$$

$$[\text{Cyp}] = \begin{cases} k_{\text{deg}} \left[\frac{\gamma(\text{RA})_{\text{signal}}}{\gamma(\text{RA})_{\text{signal}} + 1 + f_o e^{-\lambda(x_f - x)}} \right] & 0 < x < x_f - 40 \\ k_{\text{max}} & x < 0 \text{ or } x_f - 40 < x < x_f \end{cases}, \quad (3)$$

and

$$\text{RA}_{\text{signal}} = ([\text{RA}]_{\text{in}})^2 \quad (4)$$

Each variable was defined according to that provided by White et al.³² [RA]_{out} and [RA]_{in} denote the extracellular and

intracellular concentrations of RA, respectively, and [RA]_{signal} represents the intensity of RA signal transduction into the cell. *V*(*x*) denotes the rate of RA generation at position *x*. In addition, [Cyp] indicates the intracellular concentration of Cyp26a1. The parameters used are also consistent with the values previously provided³² and are as follows: *k_p* represents a first-order permeability coefficient, *D* denotes the effective extracellular diffusion coefficient of RA, and *k_{deg}* signifies the degradation constant of intracellular RA. The steady-state solutions of the equations were obtained numerically using Mathematica software. In this model, we made two assumptions: first, *V*(*x*) = 0 when exogenous RA is added, indicating no induction of RA by *aldh1a2*; and second, *k_{deg}* decreased with the addition of BPA, suggesting that BPA down-regulates *cyp26a1* activity in the hindbrain region. Mathematica simulation codes are available at https://github.com/gpr120/RA_gradient_model.

RNA Isolation, cDNA Library Construction, and Sequencing

Total RNA was isolated from individual embryos at 24 hpf ($n = 6$ embryos per group) using NucleoSpin RNA XS (No. 740902.50; Macherey-Nagel). RNA quality was assessed using NanoDrop (Thermo Fisher Scientific), PicoGreen (No. R11491; Invitrogen), and an Agilent 2100 Bioanalyzer. High-quality samples were used to construct cDNA libraries using the SMARTer Ultra-low input RNA kit (No. 634940; Takara Bio). Libraries were sequenced with paired ends using the Illumina HiSeq 2500 platform at Macrogen (Tokyo, Japan). RNA isolation, cDNA library construction, and sequencing were performed twice, with three embryos analyzed per experimental condition. Samples 1–3 and 4–6 were treated separately for RNA isolation and sequencing but analyzed together.

Transcriptome Analysis of Zebrafish

RNA-seq data were obtained by Macrogen. Raw reads in FASTQ format were assessed for quality control using FastQC (version 0.11.9).³³ Low-quality data were trimmed based on the FastQC results using Trimmomatic (version 0.39).³⁴ The cleaned reads were then mapped to the zebrafish reference genome (GCF_000002035.6_GRCz11) using STAR aligner (version 2.7.6a).³⁵ Gene-level quantification was performed using RSEM (version 1.3.3).³⁶

Analysis of normalized values for differential gene expression was conducted with the R package TCC (version 1.28.0),³⁷ applying the trimmed mean of the M-values method for normalization to ensure robust standardization. The raw transcriptome data are available in the SRA database (BioProject Accession No. PRJNA1097246; available at <https://github.com/gpr120/hiPSC-Zebrafish-exprs>).

Visualization of Differential Gene Expression by Gene Set Enrichment Analysis

To investigate the ontology of DEGs identified in both the RNA-seq and microarray analyses, we performed gene ontology (GO) enrichment analysis using the Bioconductor packages GStats and GSEA-Base. Enrichment of GO terms was assessed using Fisher's exact test to identify statistically significant differences in over- or underrepresented GO terms in comparison with the overall GO term distribution. Hierarchical clustering was performed using Ward's method, with linkage distances calculated based on correlation coefficients between samples or GO terms. R scripts used for analysis are publicly available at <https://github.com/gpr120/hiPSC-Zebrafish-exprs>.

Z-Score Normalization and Clustering for Gene Expression Profiling

A heatmap was generated to visualize the expression patterns of the targeted genes based on the z-scores, which were calculated by standardizing the expression level of each gene to a mean of 0 and a standard deviation (SD) of 1. Hierarchical clustering on the gene axis was performed using Ward's method, which effectively grouped genes with similar expression profiles.

Results

Expression of HOX Genes in Human iPSCs Coexposed to BPA and RA

Coexposure of iPSCs to 100 nM RA and various doses of BPA (2.5–20 μ M) resulted in higher expression of *HOX* genes (*HOXA1*, *HOXA2*, *HOXB1*, *HOXB2*, and *HOXB4*), in a dose-dependent manner, in comparison with that induced by RA alone (Figure 1A,B), with *HOXB1* and *HOXB2* exhibiting significantly higher expression (~600 times that with RA alone). After

coexposure of iPSCs to 20 μ M BPA and 100 nM RA, *HOXB1* and *HOXB2* expression was similar to that with 500 nM RA alone, on days 3, 4, and 5 (Figure 1A,B; Figure S1A). This coexposure effect of BPA and RA was observed even when lower concentrations of RA (10 nM and 25 nM) were used, whereas *HOX* gene expression in iPSCs was scarcely detectable or not detectable in the presence of RA alone at the lower doses (Figure 1B).

OTX2, which showed low expression in human iPSCs after exposure to RA alone, showed much lower expression, in a dose-dependent manner, when iPSCs were coexposed to RA and BPA (Figure 1A,B). These results suggest that coexposure to BPA and RA may potentiate RA signaling in comparison with that exposed to the same concentration of RA alone.

Regulation of the Induced HOX Gene Expression by RAR Antagonists

Addition of the pan-antagonist BMS493 blocked the expression of *HOX* genes in a dose-dependent manner (Figure S1B). To further investigate the potentiation effect of coexposure to BPA and RA,

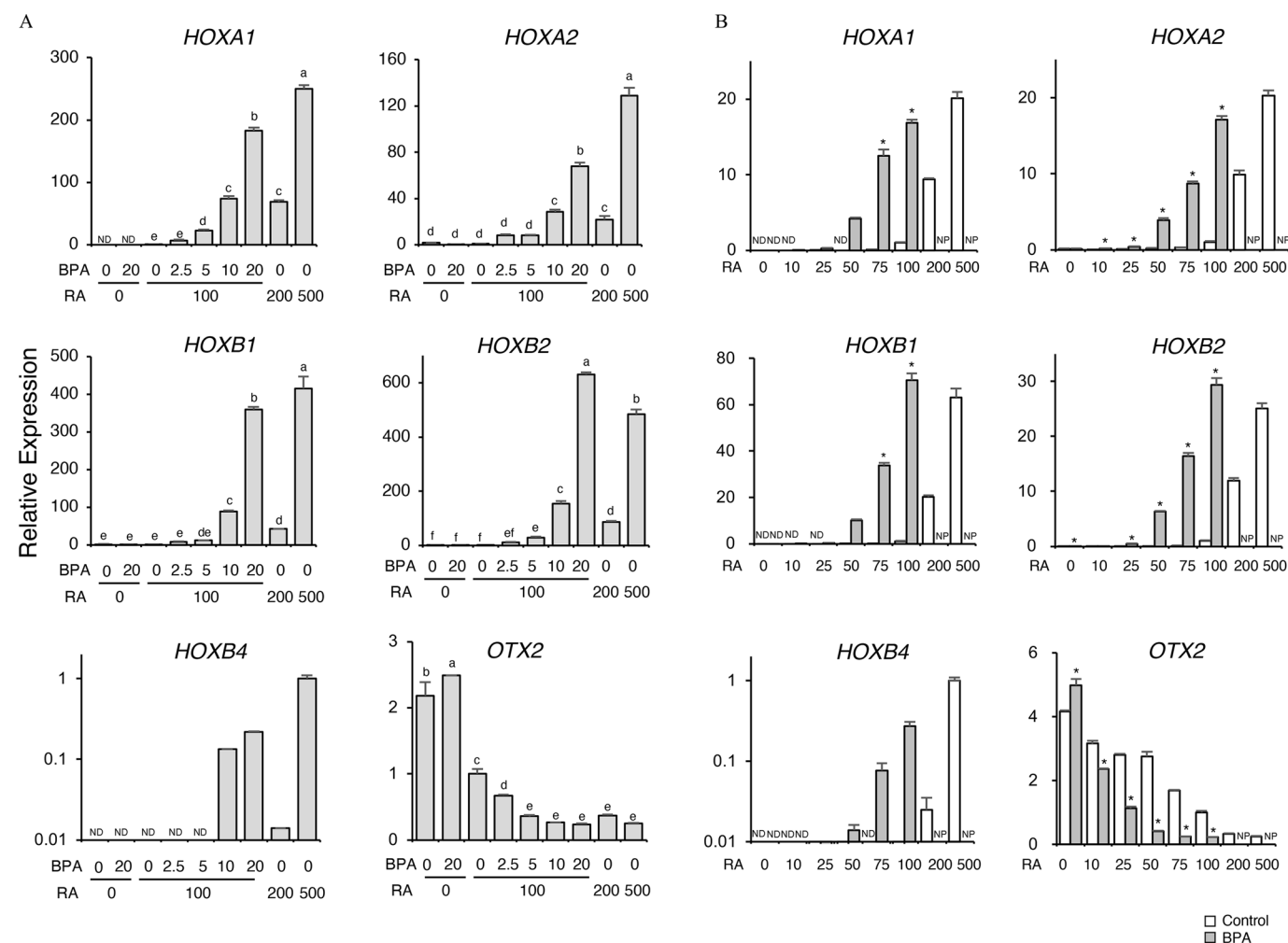


Figure 1. Expression of *HOX* genes in iPSCs coexposed to BPA and RA. (A) Gene expression (normalized to *GAPDH*) assessed by RT-qPCR in iPSCs treated with RA (0, 100, 200, 500 nM) and BPA (0, 2.5, 5, 10, and 20 μ M) for 3 d. A one-way ANOVA with Tukey's multiple comparisons test was employed to compare the different groups on all pairwise combinations. Different superscripted letters denote significantly different values between groups at $p < 0.05$. (B) iPSCs were treated with various RA concentrations (0, 10, 25, 50, 75, 100, 200, and 500 nM) with or without 20 μ M BPA for 3 d, and gene expression was analyzed by RT-qPCR. The bar plots represent the mean value ($2^{-\Delta\Delta C_t}$) \pm SD of each sample (technical triplicates); a representative experiment ($n = 3$ biological replicates) is shown. Welch's *t*-tests were used to analyze comparisons between two groups. Values with asterisks indicate significant differences from the corresponding values exposed to RA alone ($p < 0.05$). Data are presented as mean \pm SD. Data in (A) and (B) are also presented in Excel Table S1. Note: ANOVA, analysis of variance; BPA, bisphenol A; iPSC, induced pluripotent stem cells; ND, not detected; NP, not performed; RA, retinoic acid; RT-qPCR, reverse transcription–quantitative polymerase chain reaction; SD, standard deviation.

we used the subtype-specific antagonists BMS195614 (RAR α antagonist), LE135 (RAR β antagonist), and LY2955303 (RAR γ antagonist) (Figure 2A). The addition of BMS195614 or LY2955303 resulted in lower *HOX* gene expression in iPSCs, whereas the addition of LE135 resulted in higher *HOX* gene expression in iPSCs in comparison with the control, both in the absence and in the presence of BPA with 100 nM RA, suggesting that subtypes RAR α and RAR γ were responsible for the regulation of *HOX* gene expression and RA signaling (Figure 2A).

We also investigated the role of estrogen receptors (ERs) in the coexposure experiments with BPA and RA, because BPA is known to have estrogenic effects. Antagonists of ERs and membrane-bound ERs (GPR30), namely, ICI 182,780 and G-15, did not inhibit *HOX* gene expression in iPSCs exposed to RA alone or when iPSCs were coexposed to BPA and RA (Figure 2B). These results suggest that RARs, rather than ERs, mediated the *HOX* gene expression in the presence of exogenous RA and coexposure to BPA.

Except RXR γ , the RAR and RXR subtypes were expressed in undifferentiated iPSCs (Figure S1C). Although RAR β had substantially high expression in iPSCs in both the RA alone and RA/BPA coexposure groups, RAR α showed high expression in iPSCs exposed to 500 nM RA alone, and RAR γ expression was low after exposure of iPSCs to RA alone.

We investigated HOXB1 protein expression using immunodetection, followed by flow cytometry (Figure S2). Minimal expression was observed in the control, 100 nM RA-treated, and 20 μ M BPA-treated cells. However, cells treated with both 100 nM RA and 20 μ M BPA showed high levels of HOXB1 protein, with 76.3% of cells displaying a high fluorescence intensity ($>1 \times 10^2$). This level was comparable to the proportion of cells expressing HOXB1 protein in the group treated with RA alone at 500 nM (82.9% of cells), which aligns with the observed RNA expression patterns.

Microarray Analysis of Human iPSCs

Because the *HOX* genes *A1*, *A2*, *B1*, *B2*, and *B4* showed significantly higher expression, as revealed by RT-qPCR, when human iPSCs were coexposed to BPA and RA in comparison with those exposed to RA alone, we focused on the RA-responsive genes, especially *HOX* and RA-related genes (as depicted in the heatmaps in Figure 3A–C). Up-regulation and clustering of *HOXA1*–*HOXA5* and *HOXB1*–*HOXB5* were characteristic of the groups treated with RA alone at 500 nM and RA 100 nM/20 μ M BPA. These findings are consistent with the results of the RT-qPCR analyses, suggesting that RA/BPA coexposure enhanced 3' *HOX* gene expression in comparison with that with RA alone, whereas BPA alone had no impact on *HOX* gene expression (Figure 3A).

The RA 500 nM and RA 100 nM/20 μ M BPA groups exhibited similar gene expression patterns. *MEIS1* and *MEIS2* showed higher expression and *OTX2* showed lower expression in iPSCs coexposed to BPA and RA in comparison with iPSCs exposed to either compound alone (Figure 3B). The findings showing that RAR α , RAR β , and RXR β were up-regulated and RAR γ was down-regulated in the RA 500 nM and RA 100 nM/20 μ M BPA groups were consistent with the findings from RT-qPCR analysis (Figure S1C). Expression of the RA synthesis enzyme *ALDH1A2* was slightly low in the RA 500 nM and RA 100 nM/20 μ M BPA groups in comparison with that in the DMSO control group (Figure 3C). *CRABP1*, which is primarily related to RA degradation, was low in the RA 500 nM and RA 100 nM/20 μ M BPA groups. However, expression of the RA degradation enzyme *CYP26A1* was specifically low in the RA 100 nM/20 μ M BPA group.

Regional Expression of Brain Markers in Zebrafish

Because iPSCs coexposed to BPA and RA showed higher expression of 3' *HOX* genes in comparison with iPSCs exposed to RA alone, we sought to verify its physiological significance using zebrafish embryos. Initially, we investigated the dose effect of RA on phenotypes of zebrafish embryos at 96 hpf. In embryos cultured with a narrow range of RA concentrations (5, 7.5, 10, or 12.5 nM), we observed dose-dependent increases in the development of anomalies, such as pericardial edema and curved tails (Figure S3A). This range covered $\sim 14\%$ – 96% of the anomaly rate (Figure S3B,C). Coexposure to BPA along with 7.5 nM or 10 nM RA resulted in a higher rate of anomalous embryos than exposure to RA alone, equivalent to the effects of 12.5 nM RA alone (Figure 4A and Figure S3C). Exposure to BPA alone did not induce anomalies.

The time course of these RA concentrations in the medium and embryos was measured using LC-MS/MS. The addition of BPA did not affect RA dynamics, especially in the medium (Figure S3D,E).

In iPSCs, *HOXB1* showed significant potentiation on coexposure to BPA and RA, and its expression was restricted to rhombomere 4 (r4) during hindbrain segmentation. We therefore evaluated zebrafish to understand the effects of coexposure to BPA and RA on the region-specific expression of *hoxb1a* (zebrafish ortholog of human *HOXB1*) during rhombomere segmentation. Spatial expression patterns were validated using simultaneous detection of *fgf8a* as a positional standard. Expression of *hoxb1a* was limited in r4, whereas *fgf8a* was found to be expressed in the dorsal diencephalon and midbrain–hindbrain boundary (MHB), but these two signals did not overlap (Figure S4). Exposure to RA (7.5, 10, or 12.5 nM) induced a rostral shift in *hoxb1a* expression, especially on the anterior dorsal side, in some embryos (Figure 4B). Coexposure to BPA and RA further increased the number of embryos that showed such a rostral shift. We also detected *otx2b*, a midbrain marker, and noted compression of the region that was coexposed to RA and BPA (Figure 4C).

To investigate the relative regions of *hoxb1a* expression, we visualized r3 and r5 using immunostaining for *egr2b* (red) and *hoxb1a* (blue) simultaneously (Figure 4D). In RA-treated and RA/BPA-treated embryos, *hoxb1a*-expressing cells appeared to have invaded the dorsal central position of r3 and pushed aside cells expressing *egr2b* in r3.

To evaluate the effect of coexposure to BPA and RA quantitatively, we measured the linear distances between signals. The measured lengths included the distance from the dorsal diencephalon (*fgf8a*) to the anterior border of the dorsal expression of *hoxb1a* signal (dien-r4a) (Figure 4E), from the diencephalon (*fgf8a*) to the MHB (*fgf8a*) (dien-mhb) (Figure 4F), and from the MHB (*fgf8a*) to the posterior border of r4 (*hoxb1a*) (mhb-r4p) (Figure 4G). Exposure to RA at 7.5, 10, or 12.5 nM shifted *hoxb1a* expression anteriorly in a dose-dependent manner, and coexposure to RA and BPA, such as RA 7.5 nM/20 μ M BPA and RA 10 nM/20 μ M BPA, further enhanced this effect considerably in comparison with that with RA alone (Figure 4E–G). However, BPA alone had no significant effect. The lengths in the RA 7.5 nM/20 μ M BPA and RA 10 nM/20 μ M BPA coexposed groups were similar to that in the RA 10 nM alone and RA 12.5 nM alone groups, respectively (Figure 4E–G).

Similar trends were observed for *otx2b* (Figure 4H). A dose-dependent rostral shift of the posterior border of *otx2b* expression was observed with exposure to RA. Coexposure to BPA and RA resulted in a greater rostral shift of the posterior border than that with exposure to RA alone. As a result, the expression area of *otx2b* was reduced. A comparable rostral shift was observed for *hoxb4a* and *hoxb5a* (Figure S5A–E) in the RA 10 nM/20 μ M BPA

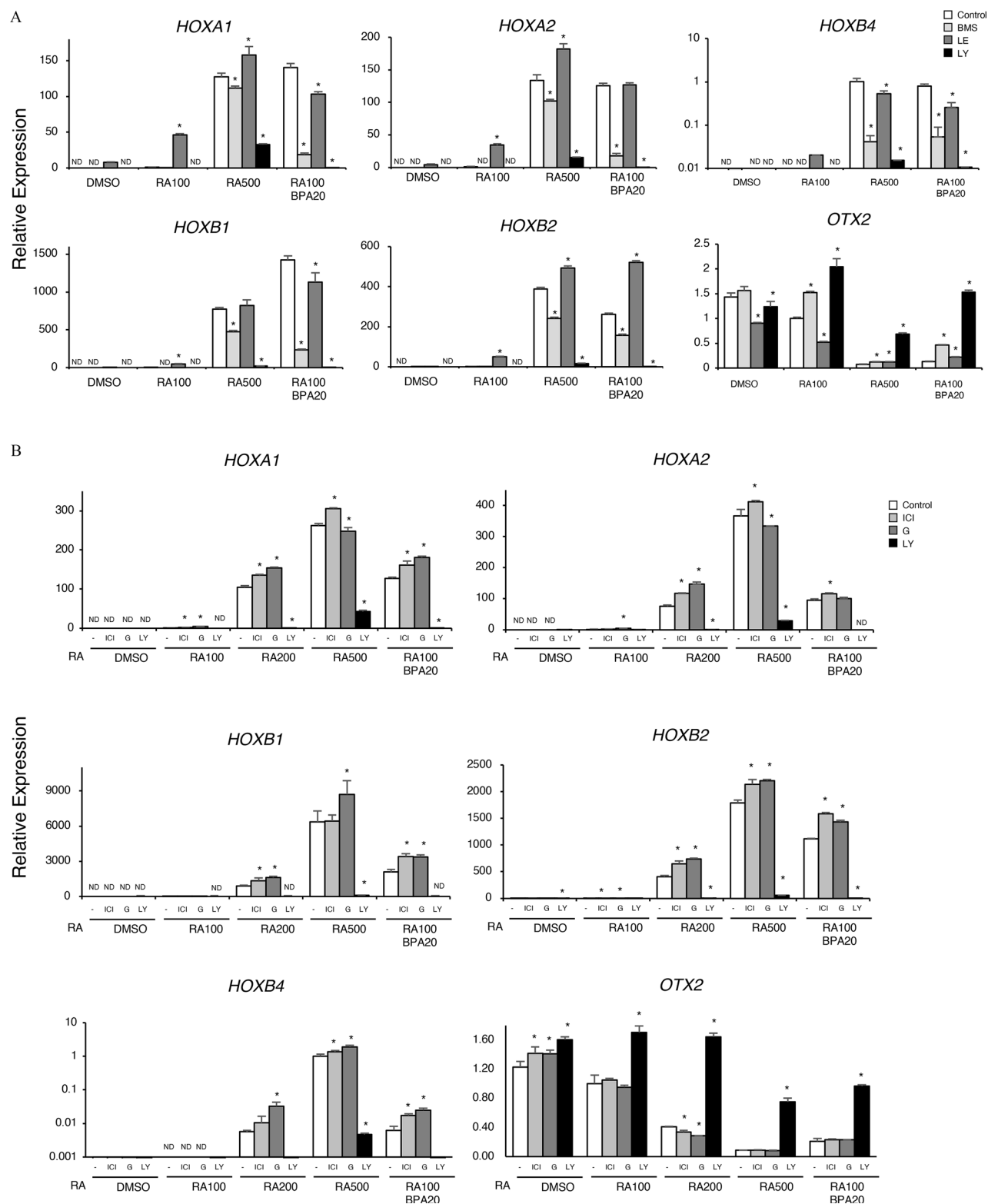
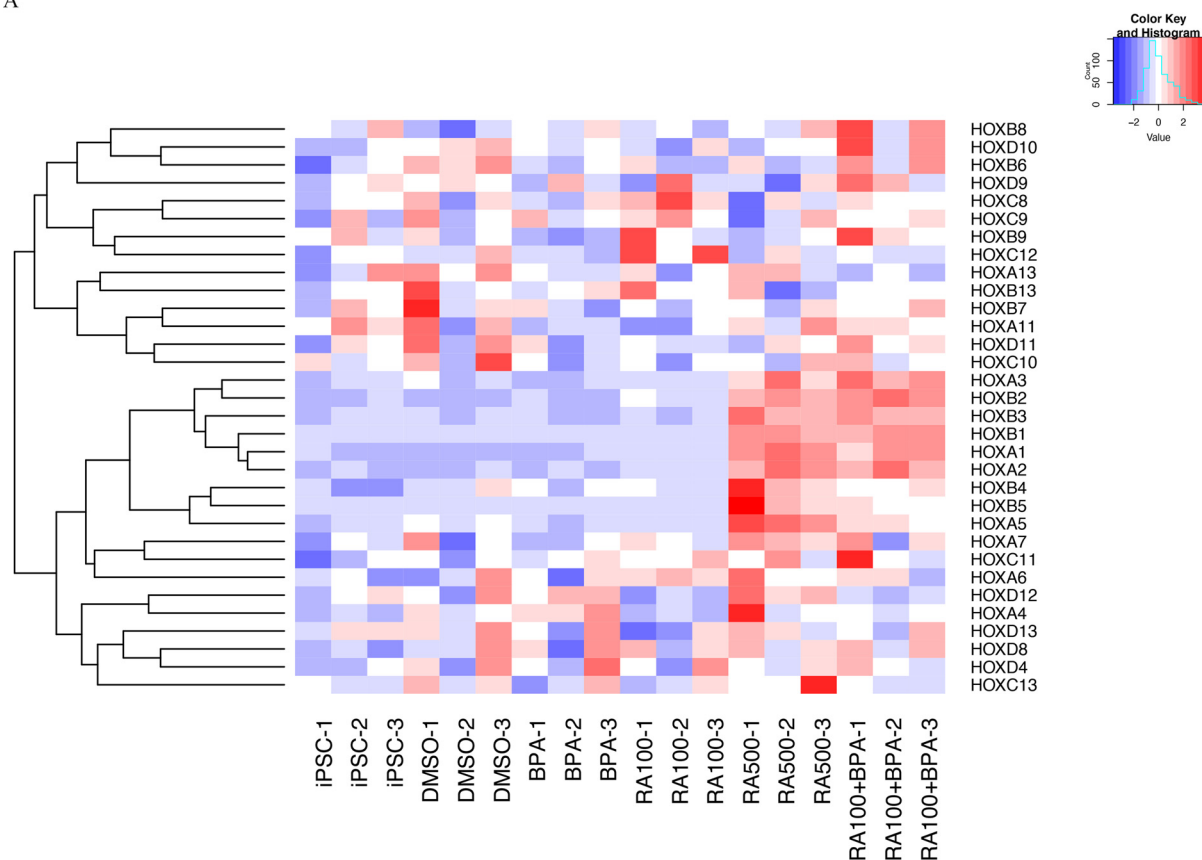
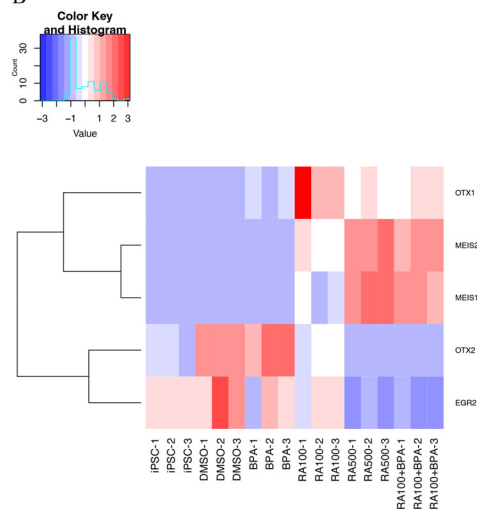


Figure 2. Repression of HOX genes by RAR antagonists. (A) Gene expression (normalized to *GAPDH*) assessed by RT-qPCR in iPSCs treated with RA (0, 100, 500 nM) and 100 nM RA plus 20 μ M BPA, in combination with RAR antagonists (100 nM BMS195614, 100 nM LE135, and 100 nM LY295303 for RAR α , RAR β , and RAR γ , respectively) for 3 d. (B) Gene expression (normalized to *GAPDH*) assessed by RT-qPCR in iPSCs treated with RA (0, 100, 200, 500 nM) or 100 nM RA/20 μ M BPA, in combination with RAR γ antagonist, 100 nM of LY295303, and ER antagonists (100 nM ICI 182,780; 500 nM G-15) for 3 d. The bar plots represent the mean value ($2^{-\Delta\Delta C_t}$) \pm SD of each sample (technical triplicates); a representative experiment ($N = 3$ biological replicates) is shown. An ANOVA with Dunnett's multiple comparisons test was employed to compare the different groups to the control group. Values with asterisks indicate significant differences from the corresponding values exposed to RA alone ($p < 0.05$). Data are presented as mean \pm SD. Data in (A) and (B) are also presented in Excel Table S2. Note: ANOVA, analysis of variance; BPA, bisphenol A; ER, estrogen receptor; iPSC, induced pluripotent stem cells; RA, retinoic acid; RAR, retinoic acid receptor; RT-qPCR, reverse transcription-quantitative polymerase chain reaction; SD, standard deviation.

A



B



C

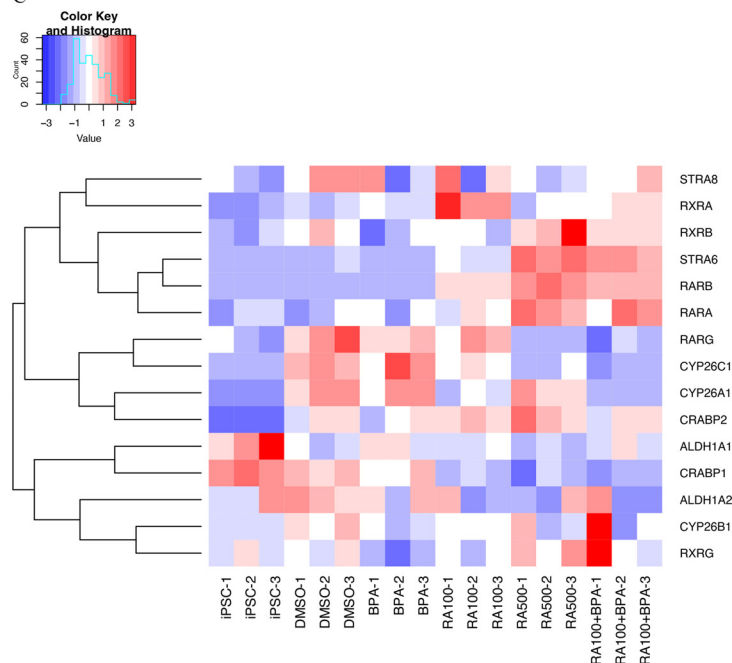


Figure 3. Microarray analysis of gene expression in iPSCs. (A) Heat map and clustering dendrogram of *HOX* genes (indicated on the horizontal axis). A heat map was generated for all iPSC samples and treatment groups (iPSCs 1–3, DMSO control 1–3, BPA 20 μ M 1–3, RA 100 nM 1–3, RA 500 nM 1–3, and RA 100 nM/20 μ M BPA 1–3). (B) Heat map and clustering dendrogram of *OTX1*, *OTX2*, *MEIS1*, *MEIS2*, and *EGR2* genes. (C) Heat map and clustering dendrogram of RA-related genes. Statistical significance was determined using Welch's analysis of variance. Changes in gene expression were considered significant at $p < 0.05$. Data in (A–C) are also presented in Excel Table S3. Note: BPA, bisphenol A; DMSO, dimethylsulfoxide; iPSC, induced pluripotent stem cells; RA, retinoic acid.

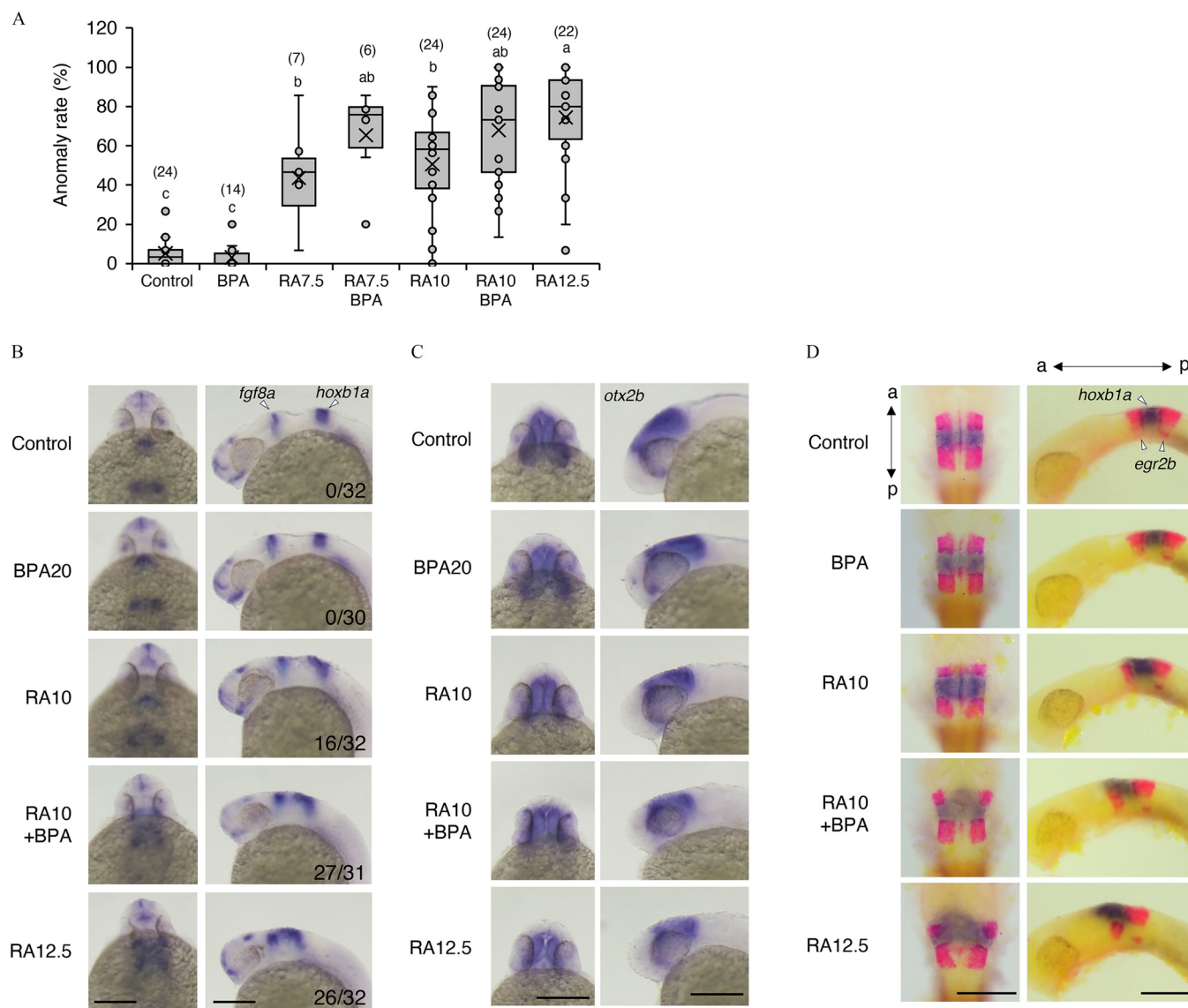


Figure 4. Effect of coexposure of zebrafish embryos to BPA and RA. (A) Anomaly rate in zebrafish larvae (96 hpf) treated with RA (0, 7.5, 10, 12.5 nM) and in combination with 20 μ M BPA for 23 h ($n=6-24$ per group; total $n=1,857$ embryos). Data represent the anomaly rate in an individual experiment (15 embryos/group). (B) Expression of *hoxb1a* and *fgf8a* as determined by WISH in 24 hpf embryos treated with RA (0, 7.5, 10, and 12.5 nM) and combined with 20 μ M BPA. Dorsal (left) and lateral (right) views are shown. The number of embryos exhibiting an obvious rostral shift in the dorsal anterior border of *hoxb1a*/total embryos is shown. (C) Expression of *otx2b* in embryos (24 hpf) treated with RA (0, 7.5, 10, and 12.5 nM) and in combination with 20 μ M BPA. Dorsal (left) and lateral (right) views are shown. (D) Expression of *hoxb1a* (blue) and *egr2b* (red) in embryos at 24 hpf. The treatment of embryos is shown on the left. Dorsal (left) and lateral (right) views are shown. (E) Linear distance between diencephalon (dien) (*fgf8a*) and the anterior border of rhombomere 4 (r4a) (*hoxb1a*) in the embryos (24 hpf) treated with RA (0, 7.5, 10, and 12.5 nM) and in combination with 20 μ M BPA. (F) Linear distance between the diencephalon (*fgf8a*) and mhb (*fgf8a*). (G) Linear distance between mhb (*fgf8a*) and the posterior border of r4 (r4p) (*hoxb1a*). (H) Length of the expression region of *otx2b*. Experiments were repeated 4 times (30 embryos/group), and a representative result is shown. The measured distance (red line) is shown in the inset picture. Scale bars: 200 μ m. (A-E-H) The boxes represent the first and third quartiles with median lines, whereas whiskers extend to the upper and lower values within $1.5 \times$ the interquartile range. The "x" symbol indicates the mean. ANOVA with Tukey's multiple comparisons test was employed to compare the different groups on all pairwise combinations. Different superscripted letters denote significantly different values between groups at $p < 0.05$. Data are presented as mean \pm SD. (I) Model of RA signaling in embryos treated with RA (0, 7.5, 10, and 12.5 nM) and in combination with 20 μ M BPA. The length represents the distance from the posterior boundary of the domain of anterior *cyp26a1* expression (approximately at the r1/r2 border). (J) Plotting of the length from the posterior boundary of the domain of anterior *cyp26a1* expression (RA signal is 0) to the position of RA signal at 250 ($y=250$, as shown in panel I) in embryos treated with RA (0, 7.5, 10, and 12.5 nM) and in combination with 20 μ M BPA. Data in (A-J) are also presented in Excel Table S4. Note: ANOVA, analysis of variance; BPA, bisphenol A; hpf, hours post fertilization; mhb, midbrain-hindbrain boundary; RA, retinoic acid; WISH, whole-mount *in situ* hybridization.

group in comparison with RA 10 nM group. An increase in signal area was also observed for *hoxb5a* (Figure S5F).

Mathematical Simulation of RA Signaling in Zebrafish

Gradient curves simulating the effects of exogenous RA exposure in zebrafish embryos were shifted toward the positive direction on the

y-axis (Figure 4I). As a result, the position that received a certain level of RA signal shifted anteriorly (Figure 4J). This finding shows good agreement with our experimental results (Figure 4B-H; Figures S4A-C and S5A-E). Furthermore, mathematical simulations demonstrated RA-dose-dependent hindbrain posteriorization and potentiation by coexposure to BPA, establishing a linear correlation between RA concentration and hindbrain rostral shift (Figure 4I,J).

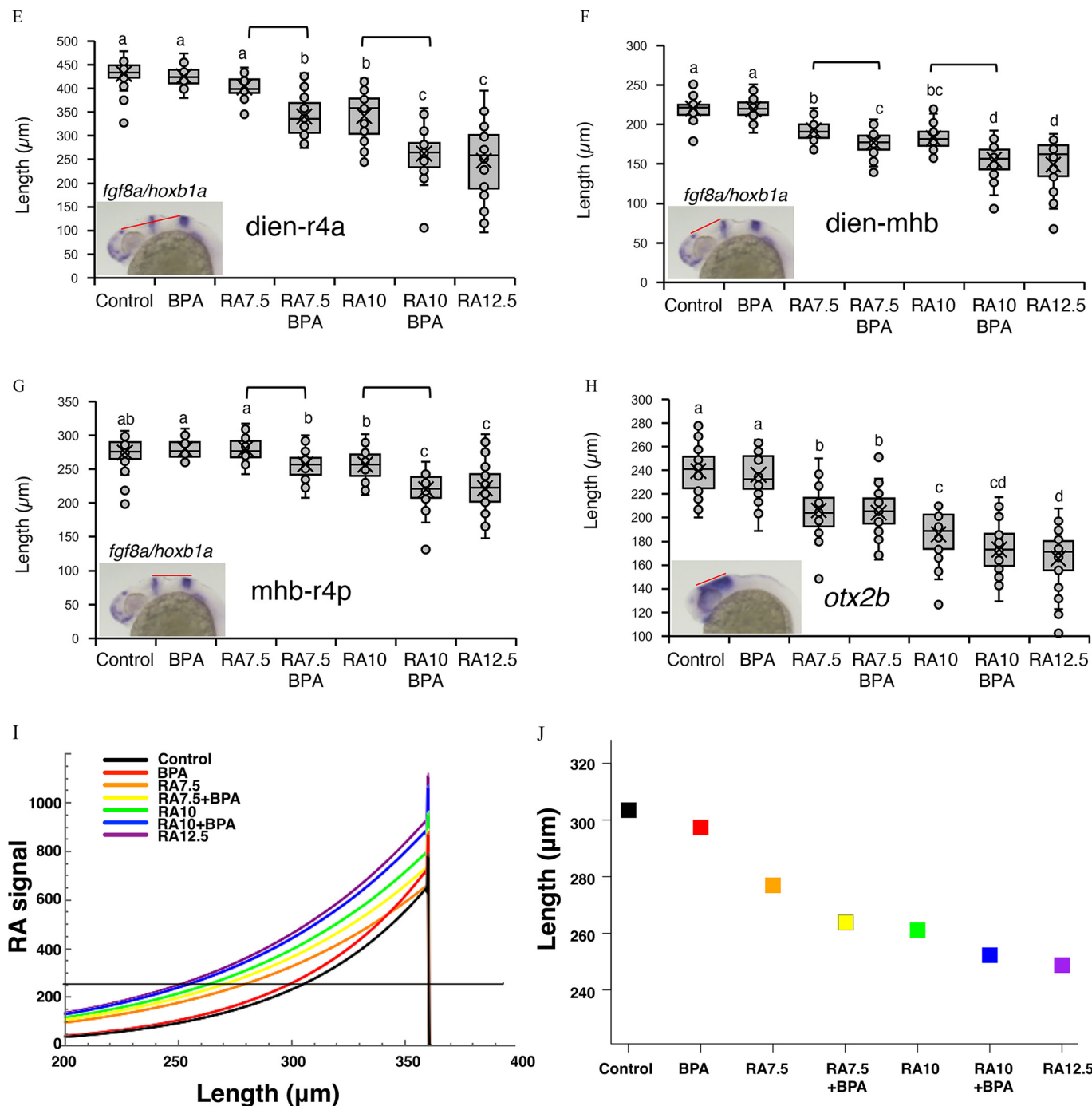


Figure 4. (Continued.)

Effect of Coexposure to BPA and RA on M-Cell Formation in Zebrafish

HOX genes are crucial in central nervous system patterning, particularly in the hindbrain, and M-cells in r4 initiate escape reflexes from startle stimuli. We explored whether coexposure of zebrafish embryos to BPA and RA potentiates RA signaling and induces M-cell duplication. Figure 5A shows varied duplication patterns, notably with axons extending to the same side of the cell body (Figure 5A, patterns D4 and D5). Analysis of M-cell anomaly rates appeared to indicate that the rates [median and interquartile range (IQR)] were increased, in a dose-dependent manner, with coexposure to BPA and RA, in comparison with that with RA alone (Figure 5B).

Effect of Coexposure to BPA and RA on Craniofacial Cartilage Formation in Zebrafish

Alcian blue staining of zebrafish embryos at 96 hpf revealed that RA exposure led to dose-dependent reductions in head size and abnormal craniofacial cartilage formation (Figure 5C,D). Coexposure to BPA and RA increased the number and severity of abnormal embryos.

Furthermore, exposure to RA increased the number of embryos in which the craniofacial cartilage was severely deformed, affecting the length (tr and oa) and angle (M-PQ and CH). Coexposure to 20 μM BPA and RA at 7.5 nM and 10 nM increased the number of anomalous embryos in comparison with exposure to RA alone

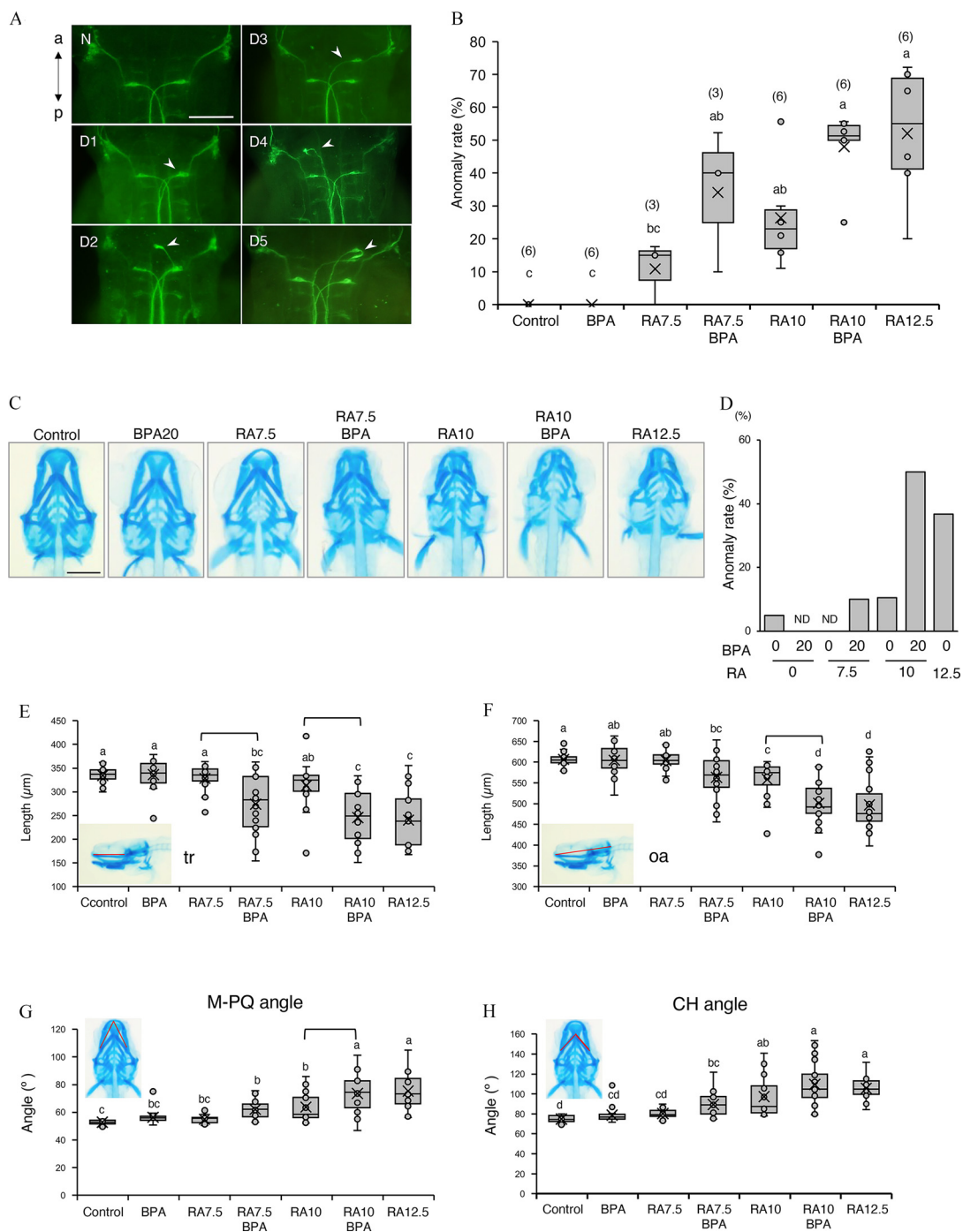


Figure 5. Effect of coexposure of zebrafish embryos to BPA and RA on neuronal cells and craniofacial cartilage. (A) Duplication of Mauthner neuronal cells induced by exogenous RA. Dorsal view of the hindbrain stained with an antineurofilament antibody. Five abnormal patterns are presented (D1–D5). N, normal; D (1–5), duplication of M-cells. Duplicated M-cells are indicated by the arrowhead. (B) Rate of anomalies in Mauthner cells in embryos treated with RA (0, 7.5, 10, and 12.5 nM) and in combination with 20 μM BPA ($n = 3–6$; total $n = 696$ embryos). Data represent the anomaly rate in an individual experiment (20 embryos/group). (C) Ventral view of craniofacial cartilage in embryos (96 hpf) treated with RA (0, 7.5, 10, and 12.5 nM) and in combination with 20 μM BPA. Anomalous embryos are shown for RA 10 nM, RA 10 nM/BPA, and RA 12.5 nM. (D) Rate of anomalies in craniofacial cartilage in embryos (96 hpf) treated with RA (0, 7.5, 10, and 12.5 nM) and in combination with 20 μM BPA. Embryos with a deformed CH, whose angle was difficult to measure, were defined as abnormal. Representative results are shown ($n = 5$). (E) Length of tr in embryos (96 hpf) treated with RA (0, 7.5, 10, and 12.5 nM) and in combination with 20 μM BPA. (F) Length of the oa in embryos (96 hpf) treated with RA (0, 7.5, 10, and 12.5 nM) and in combination with 20 μM BPA. (G) Angle of M and PQ in embryos (96 hpf) treated with RA (0, 7.5, 10, and 12.5 nM) and in combination with 20 μM BPA. (H) Angle of CH in embryos (96 hpf) treated with RA (0, 7.5, 10, and 12.5 nM) and in combination with 20 μM BPA. Experiments (20 embryos/group) were repeated 5 times, and a representative result is shown. The measured lengths and angles are indicated (red lines) in the inset. Scale bar: (A) 100 μm and (C) 200 μm. (B,E–H) The boxes represent the first and third quartiles with median lines, whereas whiskers extend to the upper and lower values within $1.5 \times$ the interquartile range. The “x” symbol indicates the mean. ANOVA with Tukey’s multiple comparisons test was employed to compare the different groups on all pairwise combinations. Different superscripted letters denote significantly different values between groups at $p < 0.05$. Data in (A–H) are also presented in Excel Table S5. Note: ANOVA, analysis of variance; BPA, bisphenol A; CH, ceratohyals; hpf, hours post fertilization; M, Meckel’s cartilage; oa, occipital arch; PQ, palatoquadrate cartilage; RA, retinoic acid; SD, standard deviation; tr, trabecular bone.

(Figure 5D). The lengths of tr and oa in embryos coexposed to BPA and RA at 7.5 nM, and especially those coexposed to BPA and RA at 10 nM, were significantly shorter in comparison with those in embryos exposed to RA alone and became similar to the lengths of tr and oa in embryos exposed to 12.5 nM RA (Figure 5E,F). The M-PQ and CH angles were larger in embryos exposed to RA alone, and coexposure to BPA further enlarged these angles (Figure 5G,H). These results suggest that BPA stimulates RA-induced anomalies in the craniofacial cartilage of zebrafish embryos and shortens the length and widens the width of the neurocranium in comparison with embryos exposed to RA alone at the same concentration.

Dose Effect of BPA and Other Chemicals in Zebrafish

We investigated the effect of BPA at lower concentrations (2 nM–20 μ M) in zebrafish embryos (Figure S6A–C). The rate of phenotypic anomalies (median and IQR) increased dose-dependently with exposure to BPA (Figure S6A). Although multiple comparisons did not yield significant differences, a single comparison using a *t*-test revealed a significant difference in the rate of M-cell anomalies following exposure to BPA in doses as low as 2 nM (Figure S6B) ($p = 0.018$, RA 10 nM vs. RA 10 nM/BPA 2 nM), and a rostral shift occurred with BPA at a dose of 1 μ M (Figure S6C) ($p = 0.046$, RA 10 nM vs. RA 10 nM/BPA 1 μ M). This finding indicates that BPA could exert an effect at lower concentrations, with M-cell duplication showing greater sensitivity than the rostral shift of brain markers.

We then investigated the effects of LE135 and NP on zebrafish embryos. At low concentrations of LE135 (10 nM) (Figure S7A–G) and NP (1 nM and 10 nM) (Figure S8A–E), we observed a similar potentiation of the RA effect on phenotypes, *hoxb1a* rostral shift, and M-cell duplication. A notable significant difference was detected in the rostral shift between the 10 nM RA and 10 nM RA/LE135 or 10 nM RA/NP groups (Figures S7C–F and S8B–D).

Effect of Pan-RAR Antagonist BMS493 in Zebrafish

To verify the role of RA signaling in hindbrain disorganization in zebrafish, we employed the pan-RAR antagonist BMS493 to assess its impact on BPA potentiation in the presence of RA. Using 50 nM of BMS493, which did not affect the phenotype (Figure 6A), we found that the phenotypic anomalies in zebrafish embryos at 96 hpf and the rostral shift of *hoxb1a* caused by coexposure to BPA and RA were nullified, reverting to control levels (Figure 6A–E). The rate of anomalies in M-cells and craniofacial cartilage also normalized, showing no significant difference from those of the control (Figure 6F–J).

Similar results were observed with the addition of BMS493 to cultures of zebrafish embryos exposed to LE135 or NP. The rate of phenotypic anomalies in embryos at 96 hpf was similar to control levels (Figure S9A,B). In the NP group, the phenotype, rostral shift in *hoxb1a* expression, M-cell duplication frequency, and craniofacial cartilage malformation rate were normalized with the addition of BMS493 (Figure S9B–I). Specifically, the significant difference in tr and oa length and CH angle induced by coexposure to 50 nM NP was reversed with the addition of BMS493 (Figure S9G–I). These findings suggest that RAR is pivotal in this signaling pathway in zebrafish.

Transcriptome Analysis in Zebrafish

Single-embryo RNA-seq analysis of transcriptomes in zebrafish was performed. Heat map and clustering analysis of *hox* genes indicated high expression of the 3' *hox* genes in the RA 12.5 nM and RA 10 nM/20 μ M BPA groups in comparison with that in

the RA 10 nM and DMSO control groups, with no effect on the 5' *hox* genes (Figure 7A). Expression of *otx1*, *otx2a*, and *otx2b* was lower in the RA 10 nM/20 μ M BPA-treated embryos (Figure 7B). The RA 12.5 nM and RA 10 nM/20 μ M BPA groups exhibited high expression of *cyp26a1*, *rxrga*, and *rxrgb*, along with low expression of *aldh1a2* in comparison with that in the RA 10 nM and control groups. In embryos coexposed to RA 10 nM and 20 μ M BPA, expression of *crabp2a* was higher and expression of *stra6*, *rarab*, and *rarga* was lower than in the RA 10 nM and control groups (Figure 7C).

To identify biological processes that might be commonly affected by coexposure to RA and BPA in both *in vitro* and *in vivo* conditions, we performed GO-based gene set enrichment analysis and selected five characteristic clusters associated with similar biological functions, showing enrichment of DEGs in both iPSCs and zebrafish embryos (Figure 7D). Cluster I consisted of the anterior/posterior pattern specifications and retinoid metabolic processes related to the retinoid system. Cluster II encompassed the development process. Cluster III comprised the central nervous system, head, and brain. Cluster IV consisted of many organs, including the heart, glands, digestive system, and nervous system. Cluster V was associated with skeletal system development. In contrast, many other clusters exhibited gene expression changes primarily in only one condition (either *in vitro* or *in vivo*), with limited overlap observed between the two.

Discussion

The findings presented in this study provide experimental evidence that human iPSCs and zebrafish embryos coexposed to BPA and RA at a specific concentration had higher expression of 3' *HOX* genes in comparison with those exposed to RA alone. As *HOX* genes and RA signaling play important roles in various fundamental biological processes, these results may explain why BPA coexposure was associated with various adverse outcomes as well as developmental neurotoxicity.

In this study, we expanded our previous work¹⁶ to investigate whether coexposure to BPA and RA would induce higher *HOX* gene expression in human iPSCs and zebrafish embryos in comparison with exposure to RA alone. Initially, we investigated the *in vitro* condition using human iPSCs and found that iPSCs coexposed to BPA and RA had higher *HOX* gene expression and lower expression of *OTX2* than that in cells exposed to RA alone (Figure 1A,B), suggesting that coexposure to BPA potentiated the RA signaling that had been stimulated by the exogenously added RA. Transcriptome analysis also showed up-regulation of the 3' *HOX*, *MEIS1*, and *MEIS2* genes and down-regulation of the *OTX2* gene in these groups (Figure 3A,B),^{38,39} which is consistent with the potentiation of RA signaling.

The region-specific expression of *HOX* genes is crucial during hindbrain formation,^{40,41} and RAR γ plays a role in hindbrain and axial patterning, with its loss resulting in axial skeleton malformations.^{42,43} To confirm the physiological relevance of this potentiation, we examined the process of hindbrain segmentation in zebrafish by assessing the expression of brain region-specific genes. Spatial expression analysis of *hoxb1a*, *fgf8a*, and *otx2b* revealed that RA induced the posteriorization of the brain region within a narrow range of RA doses (7.5–12.5 nM) (Figure 4B–H). Coexposure of zebrafish embryos to BPA and RA potentiated the rostral shift of *hox* gene expression and the reduction in the *otx2*-expressing region (Figure 4B–H), thereby narrowing the midbrain and hindbrain regions, whereas BPA alone had no effect.

We further investigated the effects of exposures on *hoxb4a* and *hoxb5a* expression (Figure S5A–F) because these genes require higher RA concentrations than *hoxb1a* for an effect to occur. Although similar potentiation of *hoxb4a* and *hoxb5a* expression by coexposure to BPA and RA was observed,

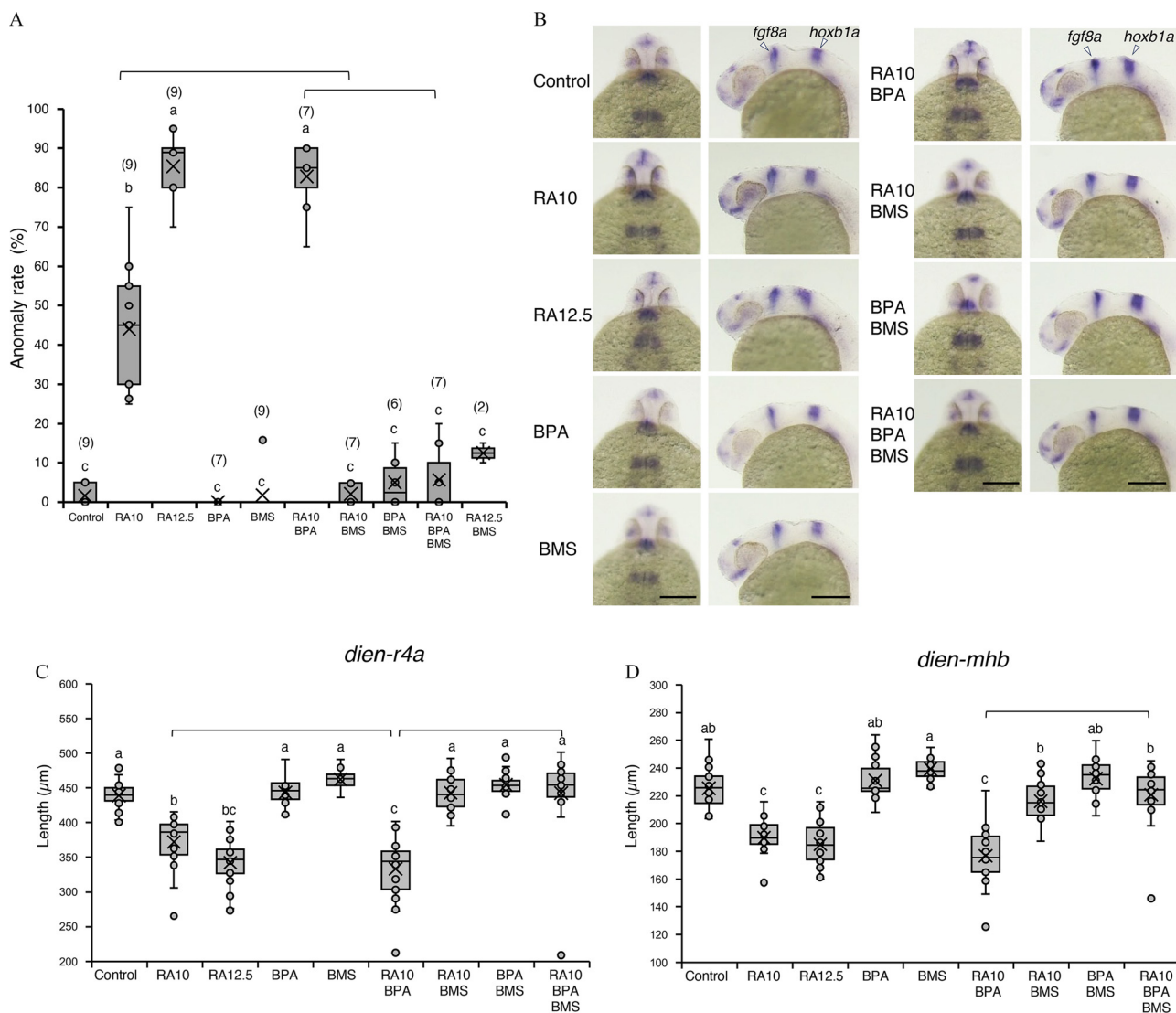


Figure 6. Effect of RAR pan-antagonist on coexposure of zebrafish embryos to BPA and RA. (A) Rate of phenotypic anomalies in zebrafish larvae at 96 hpf treated with RA (0, 10, 12.5 nM) in combination with 20 μ M of BPA, followed by addition of 50 nM BMS493 ($n=2-9$; total $n=1,427$ embryos). (B) Expression of *hoxb1a* and *fgf8a* as determined by WISH in 24 hpf embryos treated with RA (0, 10, 12.5 nM) or RA combined with 20 μ M BPA, followed by addition of 50 nM BMS493. Dorsal (left) and lateral (right) views are shown. (C) Linear distance between diencephalon (dien) (*fgf8a*) and the anterior border of rhombomere 4 (r4a) (*hoxb1a*) in embryos (24 hpf) treated with RA (0, 10, 12.5 nM) and in combination with 20 μ M BPA, followed by addition of 50 nM BMS493. (D) Linear distance between the diencephalon (dien) (*fgf8a*) and the mhb (*fgf8a*). (E) Linear distance between mhb (*fgf8a*) and the posterior border of r4 (r4p) (*hoxb1a*). (F) Rate of anomalies in M-cells in zebrafish larvae at 48 hpf treated with RA (0, 10, 12.5 nM) and in combination with 20 μ M BPA, followed by addition of 50 nM BMS493 ($n=3$; total $n=534$ embryos). (G) Length of tr in embryos (96 hpf) treated with RA (0, 10, 12.5 nM) and in combination with 20 μ M BPA, followed by addition of 50 nM BMS493. (H) Length of the oa in embryos (96 hpf) treated with RA (0, 10, 12.5 nM) and in combination with 20 μ M BPA, followed by addition of 50 nM BMS493. (I) Angle of M and PQ in embryos (96 hpf) treated with RA (0, 7.5, 10, 12.5 nM) and in combination with 20 μ M BPA, followed by addition of 50 nM BMS493. (J) Angle of CH in embryos (96 hpf) treated with RA (0, 10, and 12.5 nM) and in combination with 20 μ M BPA, followed by addition of 50 nM BMS493. The experiments were repeated three times in C–E, and twice in G–J. Representative results are shown (20 embryos/group). (A,C–J) The boxes represent the first and third quartiles with median lines, whereas whiskers extend to the upper and lower values within $1.5 \times$ the interquartile range. The “x” symbol indicates the mean. ANOVA with Tukey’s multiple comparisons test was employed to compare the different groups on all pairwise combinations. Different superscripted letters denote significantly different values between groups at $p < 0.05$. Data are presented as mean \pm SD. Data in (A–J) are also presented in Excel Table S6. Note: ANOVA, analysis of variance; BPA, bisphenol A; CH, ceratohyals; M, Meckel’s cartilage; mhb, midbrain–hindbrain boundary; oa, occipital arch; PQ, palatoquadrate cartilage; RA, retinoic acid; SD, standard deviation; tr, trabecular bone; WISH, whole-mount *in situ* hybridization.

exposure to BPA alone did not affect either gene, suggesting that BPA alone does not potentiate endogenous RA signaling, at least at the RA level of the hindbrain region.

Similar trends were observed in the frequency of duplication of M-cells (Figure 5A,B) and abnormal craniofacial cartilage formation (Figure 5C–H) in zebrafish embryos. Because *hox* gene expression correlates with neuronal differentiation in the hindbrain⁴⁴ and cranial neural crest cells,⁴¹ we examined reticulospinal neurons and craniofacial cartilage formation. M-cells in r4

initiate escape reflexes from startle stimuli, and exogenous RA application has been reported to duplicate M-cells in r4 or r2.⁴⁵ Coexposure to BPA and RA increased the frequency of RA-induced ectopic duplication of M-cells (Figure 5A,B). In some cases, we observed that M-cells formed in the midbrain region and their axon projections did not descend to the contralateral side, aligning with the same side of the body where the M-cells were located (Figure 5A, patterns D4 and D5). Despite normal startle behavior reported in fish with duplicated M-cells in r2,⁴⁶

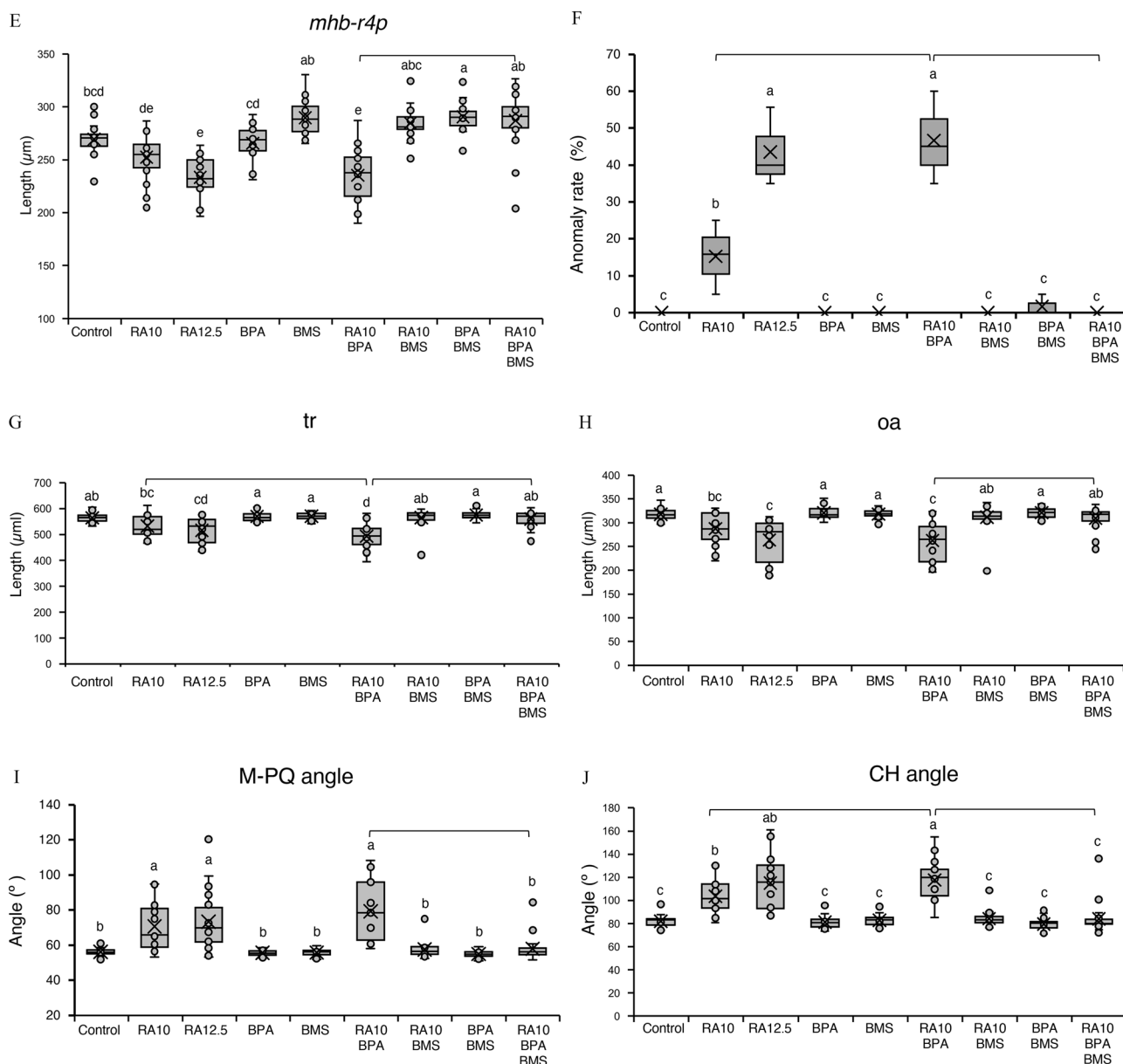


Figure 6. (Continued.)

the observed M-cells projecting axons on the same side may potentially disrupt normal startle behavior, because the stimulation signal from the extra M-cell might have transduced to the same side of the body and competed with the contralateral signal produced by the normal M-cells in r4.

Exogenous RA impacts *HOX* expression, causing malformations, especially in the hindbrain and branchial regions.⁴⁷ Meckel's cartilage and palatoquadrate arises from pharyngeal arch 1, and ceratohyal arises from pharyngeal arch 2.³⁰ The malformation of craniofacial cartilage suggests that *hox* genes expressed in cranial neural crest cells were also affected.

In the RA signaling pathway, RA regulates gene expression at the transcriptional level through nuclear RA receptors (RAR α , RAR β , and RAR γ) binding to RA response elements (RAREs) with retinoid X receptors (RXRs).¹⁷ All effects of BPA on potentiation of *HOX* genes, the brain region, M-cells, and craniofacial cartilage were abolished by the addition of RAR antagonists, suggesting that RAR is responsible for this potentiation in both iPSCs and zebrafish (Figure 2A,B and Figure 6).

We also observed the potentiation of RA signaling and resultant detrimental outcomes, such as posteriorization and reduction of the brain region (Figure 4E–H), M-cell duplication (Figure 5A,B), and craniofacial cartilage malformation (Figure 5C,H), when zebrafish embryos were exposed to a narrow range of exogenously added RA (7.5–12.5 nM), in a dose-dependent manner. Hindbrain patterning is controlled by region-specific expression of *hox* genes, tightly regulated by the endogenously formed RA gradient.^{40,41} This gradient is initially generated by RA in the somatic mesoderm produced by *aldh1a2* and diffuses through the neuroectoderm. Diffused RA is degraded by *cyp26a1* expressed in the anterior neural plate during gastrulation. The formation of a linear RA gradient during hindbrain development, with the highest concentration estimated at 6 nM,⁴⁸ aligns with our observation of a linear response within a narrow RA dose range.

To further verify this linear response, we simulated the effects of RA and BPA using a mathematical model that predicts the establishment of an RA gradient.³² In this model, the *x*-intercept value decreased in an RA-dose-dependent manner, causing the

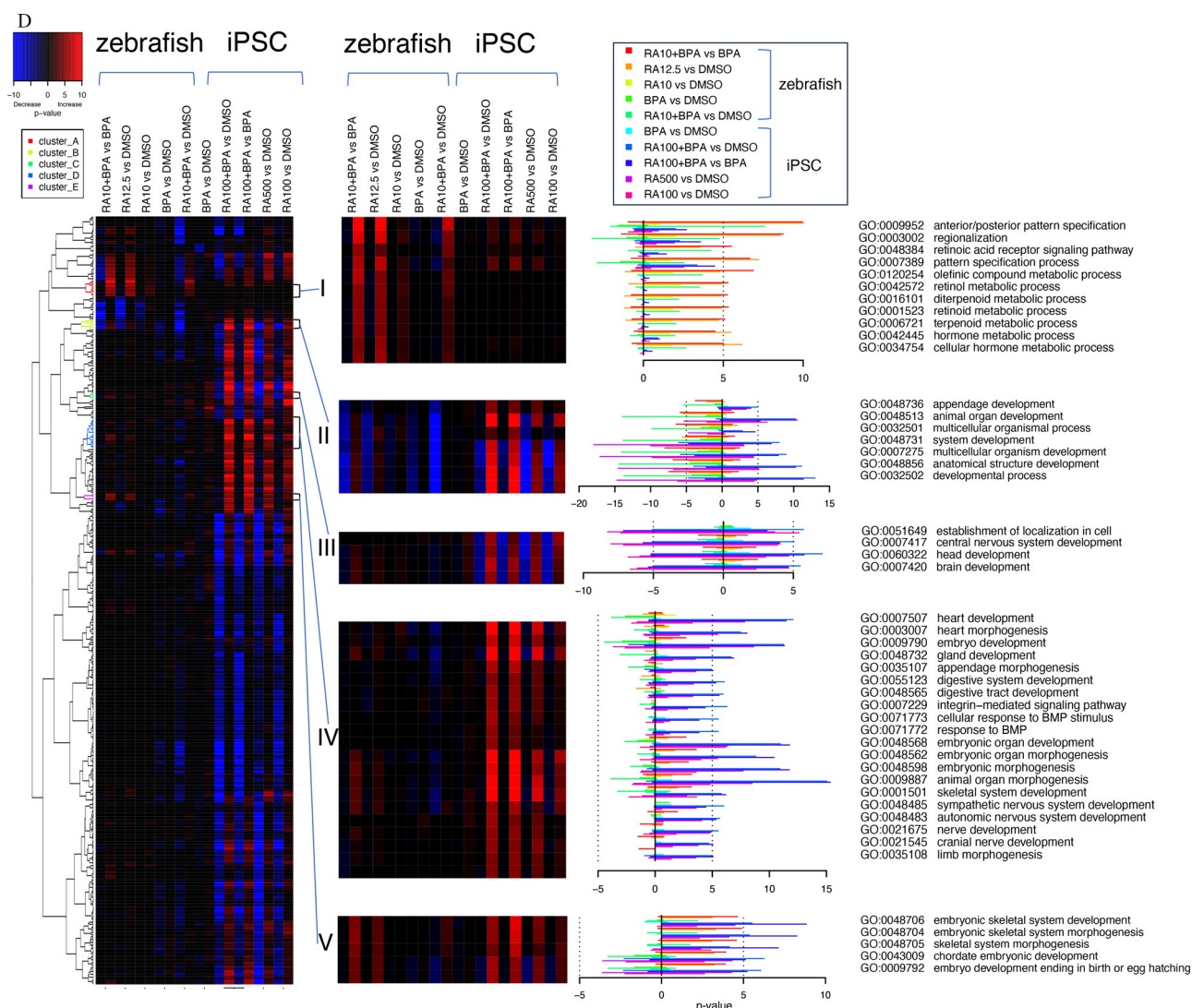


Figure 7. (Continued.)

anterior shift of RA signal position to surpass a threshold necessary for expressing specific 3' *hox* genes. This shift to anterior positions is induced by the exogenous addition of RA and coexposure to RA and BPA. Consequently, *hox* genes, such as *hoxb1a*, *hoxb4a*, and *hoxb5a*, were activated at more anterior positions, causing a rostral shift in their expression and posteriorization of the brain, resulting in a reduction of the midbrain and hindbrain regions. This model aligns well with the observed rostral shift caused by exogenously added RA and coexposure to RA and BPA. This suggests that exogenously added RA and BPA affects the endogenously formed RA gradient in early gastrula, thereby determining brain regionalization in the later stages of development (Figure 4I,J).

Regarding the assumptions we made for this modeling, repression of *aldh1a2* by the addition of RA has already been described.^{32,49,50} We validated the second assumption using WISH to verify the expression of *cyp26a1* in the brain. The signal intensity of *cyp26a1*, which was expressed in the presumptive midbrain and hindbrain regions in zebrafish embryos exposed to BPA, showed significantly lower signal intensity in comparison with that in the control group (Figure S10A,B). Therefore, the experimental results showed good agreement with the assumptions used in this simulation.

After establishing potentiation of the RA effect by BPA at a pharmacological concentration (20 μ M), we investigated the effects of a lower dose of BPA in zebrafish.⁵¹ In iPSCs, we observed enhanced expression of *HOX* genes at 2.5 μ M of BPA (Figure 1A). A significant difference in the M-cell anomaly rate was observed following coexposure to 2 nM BPA, suggesting that developmental neurotoxicity might occur at a very low concentration of BPA. Furthermore, we observed a rostral shift of *hoxb1a* and duplication of M-cells in the presence of other chemicals, such as LE135 and NP, in the 1–10 nM range (Supplementary Figures S7A–G and S8A–E). These findings suggest that these chemicals likely share a similar mechanism that is linked to adverse outcomes. The potentiation of RA's effect has also been observed in polycyclic aromatic hydrocarbons contaminating the environment.⁵² Although that study assessed hydrocarbons using *in vitro* reporter assays, the results, combined with ours, suggest that the potentiation of RA signaling might not be limited to BPA but could be a relatively common feature of various chemicals. Retinoids, which are crucial human nutrients, can be obtained from food, dietary supplements, and medicines. Environmental reports indicate contamination by RA and RA-like activity.^{22,23,53} Therefore, the effect of coexposure to chemicals and RA needs to be investigated further.

Although BPA has been reported to interact with the ER,^{10,12,14} our findings reveal that in the presence of exogenous RA, BPA promoted RA-responsive genes via RAR receptors, particularly up-regulating 3' *HOX* gene expression. However, the detailed mechanism by which coexposure to BPA potentiates RA signaling remains unclear. BPA alone did not affect 3' *HOX* gene expression in human iPSCs and zebrafish embryos, suggesting that BPA does not affect endogenous RA signaling. The reason for the lack of impact of BPA on the endogenous RA gradient in the hindbrain, especially in zebrafish, remains unclear. One possible explanation is that the level of endogenous RA is low. RA was not detected by LC-MS/MS in control embryos at any sampling time (Figure S3E). If the endogenous RA concentration in the hindbrain was increased to a level similar to that of exogenous RA at 7.5 nM, up-regulation of *hox* genes might be observed with exposure to BPA alone. Some chemicals, such as dioxin,⁵⁴ ethanol,⁵⁵ and herbicides,⁵⁶ have been reported to increase the endogenous RA level or interact with RAR. Therefore, coexposure to BPA along with these chemicals might enhance 3' *hox* gene expression without the presence of exogenous RA. Future studies will be needed to investigate this possibility.

The potentiation of RA signaling was observed both in iPSCs and in zebrafish embryos and was also observed in the presence of other chemicals such as LE135 and NP. This observation suggests that a more generalized mechanism might be responsible for this potentiation. For example, coexposure to BPA might enhance RA transportation into the cell and nuclei. Synergistic activation of RA-responsive genes has been reported by binding of the retinoid X receptor (RXR) ligand to RXR in combination with liganded RAR.⁵⁷ These possibilities need to be addressed, although BPA, NP, or LE135 are unlikely to act as ligands of RXR.

RA levels are associated with altered behavior, contributing to cognitive disorders such as ASD, age-related dementia, and Alzheimer disease.⁵⁸ Mutations in *HOXA1*, *HOXA2*, *HOXB1*, and *TALE* transcription factor are related to impaired brain stem, inner ear, cardiovascular, and cognitive development, including ASD.^{59–62} Therefore, the potentiation of 3' *HOX* genes and RA signaling could be linked to the pathogenesis of ASD and ADHD through the process of developmental neurotoxicity. Effects on neurogenesis affecting circadian rhythms have been reported with low-dose gestational exposure to BPA.⁶³ In this case, coantagonism of both estrogen and androgen receptors was required to block the effects of BPA. Because the fact that EDCs, including BPA, affect multiple signaling pathways,¹⁵ depending on the exposure conditions, it would be important to use well-defined experimental conditions that focus on the specific signaling pathway to elucidate the mechanism.

Our transcriptome analyses showed that, with coexposure to BPA and RA, expression profiles were similar between iPSCs and zebrafish, especially the 3' *HOX* gene expression responsible for hindbrain formation and the *OTX2* expression responsible for forebrain and midbrain formation (Figures 1–3; Figure 7). This result is the first evidence of BPA potentiating RA signaling on coexposure to RA, in both *in vitro* and *in vivo* settings. The observed RA potentiation at the early developmental stage, mediated through 3' *HOX* genes, suggests potential impacts on various biological processes, such as cell proliferation, differentiation, morphogenesis, reproductive system functioning, immune system functioning, neurodevelopment, metabolic function, and homeostasis,^{17,18,64–66} implying good agreement with the observed pleiotropic effects of BPA.^{9,15,67}

We compared the similarity of these transcriptomes using GO-based gene set enrichment analysis and identified five characteristic clusters associated with anterior/posterior patterning (Figure 7D, cluster I), developmental process, central nervous system development,

brain development, nerve development (cluster II, III, IV), and embryonic skeletal system development (cluster V). These were highly related to the anomalies observed in zebrafish, such as malformations of the body, heart, brain, M-cells, and craniofacial cartilage. Therefore, the cause of these anomalies was supported by changes in transcription. Moreover, this result suggests that *in vitro* differentiation using iPSCs showed a DEG expression pattern similar to that detected in zebrafish embryos.

In conclusion, all of the data obtained in this study were consistent with the notion that coexposure to BPA and RA potentiates RA signaling. We therefore propose that RA signaling is the mechanism linking chemical exposure and divergent adverse outcomes. Although BPA did not activate endogenous RA signaling by itself, it potentiated exogenous RA signaling when provided together with RA. This effect was observed in both iPSCs and zebrafish embryos and extended beyond BPA. Mathematical modeling effectively elucidated the impact of BPA on the formation of RA gradients and the rostral shift of brain markers. Our results demonstrate the potential risk posed by simultaneous exposure to BPA and RA. Even when the environmental level of RA is low and not at a level to cause anomalies, its presence might lead to diverse adverse outcomes in combination with chemicals. Moreover, analysis of its effects in the iPSC model could help effectively predict these detrimental effects, offering valuable insights into potential risks.

We performed experiments multiple times using a large number of zebrafish embryos (more than 30,000) to obtain reproducible results in *in vivo* experimental conditions. However, the detailed mechanism underlying the potentiation of RA signaling by the coexposure to BPA and RA still remains unclear. Further studies should focus on the interaction of chemicals with liganded RAR not only to provide insights into the potential of these chemicals to cause endocrine disruption, but also to elucidate the mechanism of RA signaling in these processes.

Acknowledgments

The authors thank all the laboratory members, especially Mayuko Mori, Haruna Kato, and Kazuki Yoshimura (Ritsumeikan University) for their technical contribution. The authors also would like to thank Ms. Lesley W. Allen for her dedicated developmental editing of this manuscript.

This study was funded in part by a Grant-in-Aid for Challenging Exploratory Research (17K20049 to T.T.).

T.N. performed PCR, WISH, immunostaining, sample preparation for RNA-Seq experiments, and data analysis and contributed to manuscript elaboration. T. Taya, Y.M., H.K., S.K., and T. Takada performed the iPSC culture and PCR analysis. S.K. performed the flow cytometry experiments. S.O., M.O., M.N., T.K., M.S., and M.T. performed the WISH and/or immunostaining, and subsequent measurements. S.H. and T. Tanaka conducted and supervised the statistical analyses. A.Y. and I.T. provided technical input for the iPSC experiment. Y.O. and H.J. performed LC-MS/MS analysis. N.T. performed the Alcian blue staining and measurements. A.H. performed mathematical simulation for the modeling of RA gradient formation. K.U. and A.H. conducted and supervised bioinformatics analyses. M.H., N.S., M.W., I.T., A.Y., A.I., and K.I. contributed to technical input, data analysis, and discussion. T. Takada conceived the project with additional input from A.H., performed and supervised the experiment and data analysis, and wrote the manuscript with suggestions from other authors.

References

- Vandenberg LN, Hauser R, Marcus M, Olea N, Welshons WV. 2007. Human exposure to bisphenol A (BPA). *Reprod Toxicol* 24(2):139–177, PMID: [17825522](https://doi.org/10.1016/j.reprotox.2007.07.010), <https://doi.org/10.1016/j.reprotox.2007.07.010>.

2. Chapin RE, Adams J, Boekelheide K, Gray LE, Hayward SW, Lees PSJ, et al. 2008. NTP-CERHR expert panel report on the reproductive and developmental toxicity of bisphenol A. *Birth Defects Res B Dev Reprod Toxicol* 83(3):157–395, PMID: 18613034, <https://doi.org/10.1002/bdrb.20147>.
3. Geens T, Neels H, Covaci A. 2012. Distribution of bisphenol-A, triclosan and n-nonylphenol in human adipose tissue, liver and brain. *Chemosphere* 87(7):796–802, PMID: 22277880, <https://doi.org/10.1016/j.chemosphere.2012.01.002>.
4. Vandenberg LN, Chahoud I, Heindel JJ, Padmanabhan V, Paumgarten FJR, Schoenfelder G. 2010. Urinary, circulating, and tissue biomonitoring studies indicate widespread exposure to bisphenol A. *Environ Health Perspect* 118(8):1055–1070, PMID: 20338858, <https://doi.org/10.1289/ehp.0901716>.
5. Nahar MS, Liao C, Kannan K, Harris C, Dolinoy DC. 2015. In utero bisphenol A concentration, metabolism, and global DNA methylation across matched placenta, kidney, and liver in the human fetus. *Chemosphere* 124(1):54–60, PMID: 25434263, <https://doi.org/10.1016/j.chemosphere.2014.10.071>.
6. Elsworth JD, Jentsch JD, VandeVoort CA, Roth RH, Eugene Redmond D, Leraneth C. 2013. Prenatal exposure to bisphenol A impacts midbrain dopamine neurons and hippocampal spine synapses in non-human primates. *Neurotoxicology* 35(1):113–120, PMID: 23337607, <https://doi.org/10.1016/j.neuro.2013.01.001>.
7. Kaimal A, Al Mansi MH, Dagher JB, Pope C, Varghese MG, Rudi TB, et al. 2021. Prenatal exposure to bisphenols affects pregnancy outcomes and offspring development in rats. *Chemosphere* 276:130118, PMID: 33714148, <https://doi.org/10.1016/j.chemosphere.2021.130118>.
8. Calhoun KC, Padilla-Banks E, Jefferson WN, Liu L, Gerrish KE, Young SL, et al. 2014. Bisphenol A exposure alters developmental gene expression in the fetal rhesus macaque uterus. *PLoS One* 9(1):e85894, PMID: 24465770, <https://doi.org/10.1371/journal.pone.0085894>.
9. Vom Saal FS, Vandenberg LN. 2021. Update on the health effects of bisphenol A: overwhelming evidence of harm. *Endocrinology* 162(3):bqaa171, PMID: 33516155, <https://doi.org/10.1210/endo/bqaa171>.
10. Ma Y, Liu H, Wu J, Yuan L, Wang Y, Du X, et al. 2019. The adverse health effects of bisphenol A and related toxicity mechanisms. *Environ Res* 176:108575, PMID: 31299621, <https://doi.org/10.1016/j.envres.2019.108575>.
11. Murata M, Kang JH. 2018. Bisphenol A (BPA) and cell signaling pathways. *Biotechnol Adv* 36(1):311–327, PMID: 29229539, <https://doi.org/10.1016/j.biotechadv.2017.12.002>.
12. Bergman ÅKE, Heindel J, Jobling S, Kidd K, Zoeller RT. 2012. State-of-the-science of endocrine disrupting chemicals, 2012. *Toxicology Letters* 211:S3, <https://doi.org/10.1016/j.toxlet.2012.03.020>.
13. Grignard E, Håkansson H, Munn S. 2020. Regulatory needs and activities to address the retinoid system in the context of endocrine disruption: the European viewpoint. *Reprod Toxicol* 93:250–258, PMID: 32171711, <https://doi.org/10.1016/j.reprotox.2020.03.002>.
14. Sonavane M. 2022. Chapter 1: classical and non-classical estrogen receptor effects of bisphenol A. In: *Bisphenol A: A Multi-Modal Endocrine Disruptor*. Gassman NR, ed. Cambridge, UK: The Royal Society of Chemistry, 1–25, <https://doi.org/10.1039/9781839166495-00001>.
15. Caporale N, Leemans M, Birgersson L, Germain P-L, Cheroni C, Borbély G, et al. 2022. From cohorts to molecules: adverse impacts of endocrine disrupting mixtures. *Science* 375(6582):eabe8244, PMID: 35175820, <https://doi.org/10.1126/science.abe8244>.
16. Aoki T, Takada T. 2012. Bisphenol A modulates germ cell differentiation and retinoic acid signaling in mouse ES cells. *Reprod Toxicol* 34(3):463–470, PMID: 22732146, <https://doi.org/10.1016/j.reprotox.2012.06.001>.
17. Cunningham TJ, Duester G. 2015. Mechanisms of retinoic acid signalling and its roles in organ and limb development. *Nat Rev Mol Cell Biol* 16(2):110–123, PMID: 25560970, <https://doi.org/10.1038/nrm3932>.
18. Ghyselinck NB, Duester G. 2019. Retinoic acid signaling pathways. *Development* 146(13):1–7, PMID: 31273085, <https://doi.org/10.1242/dev.167502>.
19. Inoue D, Sei K, Ike M. 2010. Disruption of retinoic acid receptor signaling by environmental pollutants. *J Health Sci* 56(3):221–230, <https://doi.org/10.1248/jhs.56.221>.
20. Sehnal L, Procházková T, Smutná M, Kohoutek J, Lepšová-Skácelová O, Hilscherová K. 2019. Widespread occurrence of retinoids in water bodies associated with cyanobacterial blooms dominated by diverse species. *Water Res* 156:136–147, PMID: 30909126, <https://doi.org/10.1016/j.watres.2019.03.009>.
21. Zhou GJ, Li XY, Leung KMY. 2019. Retinoids and oestrogenic endocrine disrupting chemicals in saline sewage treatment plants: removal efficiencies and ecological risks to marine organisms. *Environ Int* 127:103–113, PMID: 30909093, <https://doi.org/10.1016/j.envint.2019.03.030>.
22. Yeung KMY, Zhou GJ, Hilscherová K, Giesy JP, Leung KMY. 2020. Current understanding of potential ecological risks of retinoic acids and their metabolites in aquatic environments. *Environ Int* 136:105464, PMID: 31926435, <https://doi.org/10.1016/j.envint.2020.105464>.
23. Kubickova B, Ramwell C, Hilscherova K, Jacobs MN. 2021. Highlighting the gaps in hazard and risk assessment of unregulated endocrine active substances in surface waters: retinoids as a European case study. *Environ Sci Eur* 33(1), <https://doi.org/10.1186/s12302-020-00428-0>.
24. Lippmann ES, Estevez-Silva MC, Ashton RS. 2014. Defined human pluripotent stem cell culture enables highly efficient neuroepithelium derivation without small molecule inhibitors. *Stem Cells* 32(4):1032–1042, PMID: 24357014, <https://doi.org/10.1002/stem.1622>.
25. Lippmann ES, Williams CE, Ruhl DA, Estevez-Silva MC, Chapman ER, Coon JJ, et al. 2015. Deterministic HOX patterning in human pluripotent stem cell-derived neuroectoderm. *Stem Cell Reports* 4(4):632–644, PMID: 25843047, <https://doi.org/10.1016/j.stemcr.2015.02.018>.
26. Gentleman RC, Carey VJ, Bates DM, Bolstad B, Dettling M, Dudoit S, et al. 2004. Bioconductor: open software development for computational biology and bioinformatics. *Genome Biol* 5(10):R80, PMID: 15461798, <https://doi.org/10.1186/gb-2004-5-10-r80>.
27. Irizarry RA, Hobbs B, Collin F, Beazer-Barclay YD, Antonellis KJ, Scherf UWE, et al. 2003. Exploration, normalization, and summaries of high density oligonucleotide array probe level data. *Biostatistics* 4(2):249–264, PMID: 12925520, <https://doi.org/10.1093/biostatistics/4.2.249>.
28. Morgenstern J, Fleming T, Kliemank E, Brune M, Nawroth P, Fischer A. 2021. Quantification of all-trans retinoic acid by liquid chromatography–tandem mass spectrometry and association with lipid profile in patients with type 2 diabetes. *Metabolites* 11(1):60, PMID: 33478094, <https://doi.org/10.3390/metabo11010060>.
29. Thisse C, Thisse B. 2008. High-resolution *in situ* hybridization to whole-mount zebrafish embryos. *Nat Protoc* 3(1):59–69, PMID: 18193022, <https://doi.org/10.1038/nprot.2007.514>.
30. Strecker R, Weigt S, Braunbeck T. 2013. Cartilage and bone malformations in the head of zebrafish (*Danio rerio*) embryos following exposure to disulfiram and acetic acid hydrazide. *Toxicol Appl Pharmacol* 268(2):221–231, PMID: 23391615, <https://doi.org/10.1016/j.taap.2013.01.023>.
31. Takahashi K, Ito Y, Yoshimura M, Nikaido M, Yuikawa T, Kawamura A, et al. 2021. A globin-family protein, Cytochrome 1, is involved in the development of neural crest-derived tissues and organs in zebrafish. *Dev Biol* 472:1–17, PMID: 33358912, <https://doi.org/10.1016/j.ydbio.2020.12.016>.
32. White RJ, Nie Q, Lander AD, Schilling TF. 2007. Complex regulation of *cyp26a1* creates a robust retinoic acid gradient in the zebrafish embryo. *PLoS Biol* 5(11):e304, PMID: 18031199, <https://doi.org/10.1371/journal.pbio.0050304>.
33. Schmieder R, Edwards R. 2011. Quality control and preprocessing of metagenomic datasets. *Bioinformatics* 27(6):863–864, PMID: 21278185, <https://doi.org/10.1093/bioinformatics/btr026>.
34. Bolger AM, Lohse M, Usadel B. 2014. Trimmomatic: a flexible trimmer for Illumina sequence data. *Bioinformatics* 30(15):2114–2120, PMID: 24695404, <https://doi.org/10.1093/bioinformatics/btu170>.
35. Dobin A, Davis CA, Schlesinger F, Drenkow J, Zaleski C, Jha S, et al. 2013. STAR: ultrafast universal RNA-seq aligner. *Bioinformatics* 29(1):15–21, PMID: 23104886, <https://doi.org/10.1093/bioinformatics/bts635>.
36. Li B, Dewey CN. 2011. RSEM: accurate transcript quantification from RNA-Seq data with or without a reference genome. *BMC Bioinformatics* 12(1):323, PMID: 21816040, <https://doi.org/10.1186/1471-2105-12-323>.
37. Sun J, Nishiyama T, Shimizu K, Kadota K. 2013. TCC: an R package for comparing tag count data with robust normalization strategies. *BMC Bioinformatics* 14:219, PMID: 23837715, <https://doi.org/10.1186/1471-2105-14-219>.
38. Mahony S, Mazzoni EO, McCuine S, Young RA, Wichterle H, Gifford DK. 2011. Ligand-dependent dynamics of retinoic acid receptor binding during early neurogenesis. *Genome Biol* 12(1):R2, PMID: 21232103, <https://doi.org/10.1186/gb-2011-12-1-r2>.
39. Okada Y, Shimazaki T, Sobue G, Okano H. 2004. Retinoic-acid-concentration-dependent acquisition of neural cell identity during *in vitro* differentiation of mouse embryonic stem cells. *Dev Biol* 275(1):124–142, PMID: 15464577, <https://doi.org/10.1016/j.ydbio.2004.07.038>.
40. Alexander T, Nolte C, Krumlauf R. 2009. *Hox* genes and segmentation of the hindbrain and axial skeleton. *Annu Rev Cell Dev Biol* 25:431–456, PMID: 19575673, <https://doi.org/10.1146/annurev.cellbio.042308.113423>.
41. Parker HJ, Bronner ME, Krumlauf R. 2016. The vertebrate *Hox* gene regulatory network for hindbrain segmentation: evolution and diversification: coupling of a *Hox* gene regulatory network to hindbrain segmentation is an ancient trait originating at the base of vertebrates. *Bioessays* 38(6):526–538, PMID: 27027928, <https://doi.org/10.1002/bies.201600010>.
42. Lohnes D, Kastner P, Dierich A, Mark M, LeMour M, Chambon P. 1993. Function of retinoic acid receptor γ in the mouse. *Cell* 73(4):643–658, PMID: 8388780, [https://doi.org/10.1016/0092-8674\(93\)90246-m](https://doi.org/10.1016/0092-8674(93)90246-m).
43. Wendling O, Ghyselinck NB, Chambon P, Mark M. 2001. Roles of retinoic acid receptors in early embryonic morphogenesis and hindbrain patterning. *Development* 128(11):2031–2038, PMID: 11493525, <https://doi.org/10.1242/dev.128.11.2031>.
44. Glover JC. 2001. Correlated patterns of neuron differentiation and *Hox* gene expression in the hindbrain: a comparative analysis. *Brain Res Bull* 55(6):683–693, PMID: 11595353, [https://doi.org/10.1016/s0304-9230\(01\)00562-7](https://doi.org/10.1016/s0304-9230(01)00562-7).

45. Hill J, Clarke JDW, Vargesson N, Jowett T, Holder N. 1995. Exogenous retinoic acid causes specific alterations in the development of the midbrain and hindbrain of the zebrafish embryo including positional respecification of the Mauthner neuron. *Mech Dev* 50(1):3–16, PMID: [7605750](#), [https://doi.org/10.1016/0925-4773\(94\)00321-d](https://doi.org/10.1016/0925-4773(94)00321-d).
46. Hale ME, Kheirbek MA, Schrieffer JE, Prince VE. 2004. *Hox* gene misexpression and cell-specific lesions reveal functionality of homeotically transformed neurons. *J Neurosci* 24(12):3070–3076, PMID: [15044546](#), <https://doi.org/10.1523/JNEUROSCI.5624-03.2004>.
47. Marshall H, Morrison A, Studer M, Pöpperl H, Krumlauf R. 1996. Retinoids and *Hox* genes. *FASEB J* 10(9):969–978, PMID: [8801179](#), <https://doi.org/10.1096/fasebj.10.9.8801179>.
48. Shimozone S, Imura T, Kitaguchi T, Higashijima S, Miyawaki A. 2013. Visualization of an endogenous retinoic acid gradient across embryonic development. *Nature* 496(7445):363–366, PMID: [23563268](#), <https://doi.org/10.1038/nature12037>.
49. Schilling TF, Nie Q, Lander AD. 2012. Dynamics and precision in retinoic acid morphogen gradients. *Curr Opin Genet Dev* 22(6):562–569, PMID: [23266215](#), <https://doi.org/10.1016/j.gde.2012.11.012>.
50. Emoto Y, Wada H, Okamoto H, Kudo A, Imai Y. 2005. Retinoic acid-metabolizing enzyme Cyp26a1 is essential for determining territories of hindbrain and spinal cord in zebrafish. *Dev Biol* 278(2):415–427, PMID: [15680360](#), <https://doi.org/10.1016/j.ydbio.2004.11.023>.
51. Wetherill YB, Akingbemi BT, Kanno J, McLachlan JA, Nadal A, Sonnenschein C, et al. 2007. *In vitro* molecular mechanisms of bisphenol A action. *Reprod Toxicol* 24(2):178–198, PMID: [17628395](#), <https://doi.org/10.1016/j.reprotox.2007.05.010>.
52. Novák J, Benisek M, Pachernik J, Janosek J, Šidlová T, Kiviranta H, et al. 2007. Interference of contaminated sediment extracts and environmental pollutants with retinoid signaling. *Environ Toxicol Chem* 26(8):1591–1599, PMID: [17702330](#), <https://doi.org/10.1897/06-513r.1>.
53. Pípal M, Novák J, Rafajová A, Smutná M, Hilscherová K. 2022. Teratogenicity of retinoids detected in surface waters in zebrafish embryos and its predictability by *in vitro* assays. *Aquat Toxicol* 246:106151, PMID: [35390581](#), <https://doi.org/10.1016/j.aquatox.2022.106151>.
54. Nilsson CB, Hoegberg P, Trossvik C, Azaïs-Braesco V, Blaner WS, Fex G, et al. 2000. 2,3,7,8-tetrachlorodibenzo-*p*-dioxin increases serum and kidney retinoic acid levels and kidney retinol esterification in the rat. *Toxicol Appl Pharmacol* 169(2):121–131, PMID: [11097864](#), <https://doi.org/10.1006/taap.2000.9059>.
55. Kane MA, Folias AE, Wang FC, Napoli JL. 2010. Ethanol elevates physiological all-*trans*-retinoic acid levels in select loci through altering retinoid metabolism in multiple loci: a potential mechanism of ethanol toxicity. *FASEB J* 24(3):823–832, PMID: [19890016](#), <https://doi.org/10.1096/fj.09-141572>.
56. Paganelli A, Gnazzo V, Acosta H, López SL, Carrasco AE. 2010. Glyphosate-based herbicides produce teratogenic effects on vertebrates by impairing retinoic acid signaling. *Chem Res Toxicol* 23(10):1586–1595, PMID: [20695457](#), <https://doi.org/10.1021/bx1001749>.
57. Roy B, Taneja R, Chambon P. 1995. Synergistic activation of retinoic acid (RA)-responsive genes and induction of embryonal carcinoma cell differentiation by an RA receptor α (RAR α)-, RAR β -, or RAR γ -selective ligand in combination with a retinoid X receptor-specific ligand. *Mol Cell Biol* 15(12):6481–6487, PMID: [8524212](#), <https://doi.org/10.1128/MCB.15.12.6481>.
58. Wołoszynowska-Fraser MU, Kouchmeshky A, McCaffery P. 2020. Vitamin A and retinoic acid in cognition and cognitive disease. *Annu Rev Nutr* 40:247–272, PMID: [32966186](#), <https://doi.org/10.1146/annurev-nutr-122319-034227>.
59. Tischfield MA, Bosley TM, Salih MAM, Alorainy IA, Sener EC, Nester MJ, et al. 2005. Homozygous HOXA1 mutations disrupt human brainstem, inner ear, cardiovascular and cognitive development. *Nat Genet* 37(10):1035–1037, PMID: [16155570](#), <https://doi.org/10.1038/ng1636>.
60. Lescroart F, Zaffran S. 2018. *Hox* and *tale* transcription factors in heart development and disease. *Int J Dev Biol* 62(11–12):837–846, PMID: [30604853](#), <https://doi.org/10.1387/jidb.180192sz>.
61. Song R-R, Zou L, Zhong R, Zheng X-W, Zhu B-B, Chen W, et al. 2011. An integrated meta-analysis of two variants in HOXA1/HOXB1 and their effect on the risk of autism spectrum disorders. *PLoS One* 6(9):e25603, PMID: [21980499](#), <https://doi.org/10.1371/journal.pone.0025603>.
62. Quinonez SC, Innis JW. 2014. Human HOX gene disorders. *Mol Genet Metab* 111(1):4–15, PMID: [24239177](#), <https://doi.org/10.1016/j.ymgme.2013.10.012>.
63. Nesan D, Feighan KM, Antle MC, Kurrasch DM. 2021. Gestational low-dose BPA exposure impacts suprachiasmatic nucleus neurogenesis and circadian activity with transgenerational effects. *Sci Adv* 7(22):eabd1159, PMID: [34049886](#), <https://doi.org/10.1126/sciadv.abd1159>.
64. Samarut E, Fraher D, Laudet V, Gibert Y. 2015. ZebRA: an overview of retinoic acid signaling during zebrafish development. *Biochim Biophys Acta* 1849(2):73–83, PMID: [24928143](#), <https://doi.org/10.1016/j.bbagr.2014.05.030>.
65. Rhinn M, Dollé P. 2012. Retinoic acid signalling during development. *Development* 139(5):843–858, PMID: [22318625](#), <https://doi.org/10.1242/dev.065938>.
66. Nolte C, De Kumar B, Krumlauf R. 2019. *Hox* genes: downstream “effectors” of retinoic acid signaling in vertebrate embryogenesis. *Genesis* 57(7–8):e23306, PMID: [31111645](#), <https://doi.org/10.1002/dvg.23306>.
67. Sonavane M, Gassman NR. 2019. Bisphenol A co-exposure effects: a key factor in understanding BPA’s complex mechanism and health outcomes. *Crit Rev Toxicol* 49(5):371–386, PMID: [31256736](#), <https://doi.org/10.1080/10408444.2019.1621263>.